BRL

AD

MEMORANDUM REPORT NO. 2710

A REVIEW OF ATMOSPHERIC TRANSMISSION
INFORMATION IN THE OPTICAL AND
MICROWAVE SPECTRAL REGIONS

Alan R. Downs

December 1976

D D C

RECEIVED

FEB 1 1977

D

USA BALLISTIC RESEARCH LABORATORIES
ABERDEEN PROVING GROUND, MARYLAND

REPORT DOCUMENTATION PAGE		READ INSTRUCTIONS BEFORE COMPLETING FORM
1. REPORT NUMBER MEMORANDUM REPORT NO. 2710	2. GOV'T ACCESSION NO.	3. RECIPIENT'S CATALOG NUMBER
4. TITLE (and Subtitle) A Review of Atmospheric Transmission Information in the Optical and Microwave Spectral Regions		5. TYPE OF REPORT & PERIOD COVERED Final
		6. PERFORMING ORG. REPORT NUMBER
7. AUTHOR(s) Alan R. Downs		8. CONTRACT OR GRANT NUMBER(s)
9. PERFORMING ORGANIZATION NAME AND ADDRESS US Army Ballistic Research Laboratory Aberdeen Proving Ground, Maryland 21005		10. PROGRAM ELEMENT, PROJECT, TASK AREA & WORK UNIT NUMBERS RDTE Project No. 1W662618AH80
11. CONTROLLING OFFICE NAME AND ADDRESS US Army Materiel Development & Readiness Command 5001 Eisenhower Avenue Alexandria, Virginia 22333		12. REPORT DATE DECEMBER 1976
		13. NUMBER OF PAGES 59
14. MONITORING AGENCY NAME & ADDRESS(if different from Controlling Office) BRL-MR-2710		15. SECURITY CLASS. (of this report) UNCLASSIFIED
		15a. DECLASSIFICATION/DOWNGRADING SCHEDULE

16. DISTRIBUTION STATEMENT (of this Report)

Approved for public release; distribution unlimited.

17. DISTRIBUTION STATEMENT (of the abstract entered in Block 20, if different from Report)

18. SUPPLEMENTARY NOTES

19. KEY WORDS (Continue on reverse side if necessary and identify by block number)

Haze	Water Vapor	Microwave Transmission
Fog	Mie Scattering	Absorption
Rain	Rayleigh Scattering	
Atmospheric Transmission	Optical Transmission	

20. ABSTRACT (Continue on reverse side if necessary and identify by block number)   (kt/cs)

Much information has been generated over a long period of time on the transmission through the atmosphere of radiation of various wavelengths. This report represents an attempt to consolidate some of the available information into a single report. This report addresses five wavelengths each in the optical and microwave regions. Attenuation mechanisms considered are Rayleigh and Mie scattering and absorption by both water vapor and water drops. → next page

(Continued on reverse side).

DD ₁ FORM JAN 73 1473   EDITION OF 1 NOV 65 IS OBSOLETE

050 750

20. ABSTRACT (Continued)

Atmospheres characterized by visibilities between 0.1 km (fog) and 325 km (clear air) and by rainfalls at rates up to 64 mm/hr are considered. Pertinent formulations and tables are provided to assist in calculating attenuation coefficients characteristic of a wide variety of atmospheres, and the adequacy of the data bases upon which such calculations rest is assessed. A limited amount of information is also provided on the attenuation characteristics of smoke and dust.

TABLE OF CONTENTS

Page

LIST OF ILLUSTRATIONS

I. INTRODUCTION

The transmission through various atmospheric constituents of electromagnetic radiation of different frequencies is a very complex phenomenon. Various aspects of this phenomenon have been studied - intensively in some cases, skimpily in others - in a rather piecemeal fashion. Some basic references which treat the transmission problem from a physics standpoint do not contain the information about real atmospheres needed to make useful transmission predictions. Other references which are more system oriented often are condition-limited since atmospheric transmission is only a small part of the total problem. As a result, the available information on atmospheric transmission is not easy to find, interpret, or use. The purpose of this report is to piece together some of the known information on atmospheric transmission between the visual and millimetre wavelengths, to evaluate the quality of the available data base upon which transmission predictions rest, and to present for side-by-side comparison some transmission data at widely different wavelengths.

The two graphs presented in Figure 1 were recently published in a BRL Report.[1] These graphs summarize a large amount of work which has been done at the Ballistic Research Laboratory and elsewhere. The drawbacks of such a simplified approach are that the various sources of attenuation are not broken out adequately so that comparisons can be made between the attenuation sources, and predictions cannot be made for conditions not addressed directly on the graphs. On the other hand, the general behavior of some of the transmission parameters is readily apparent. The approach to be used in this report is the development or extraction from existing sources of an attenuation coefficient, σ, which is a function of the wavelength of the radiation and the atmospheric constituent of interest. Comparisons will then be made between the transmissions of these constituents through a specified segment of atmosphere.

It should be realized that some of the wavelength/constituent combinations rest upon a more reliable data base than do others. The following table gives a general guide to the sufficiency and/or quality of the available data.

---

[1] V.W. Richard and J.E. Kammerer, "Rain Backscatter Measurements and Theory at Millimeter Wavelengths," BRL Report No. 1838, October 1975. (AD #B008173L)
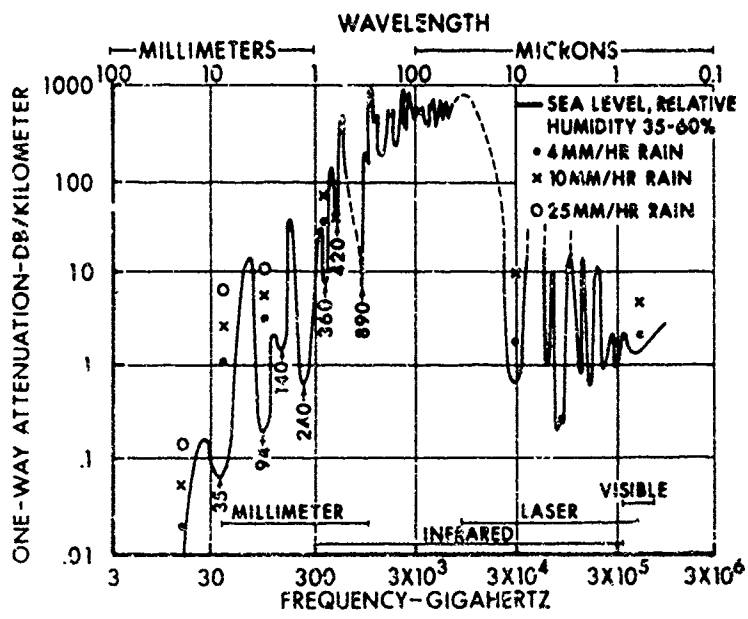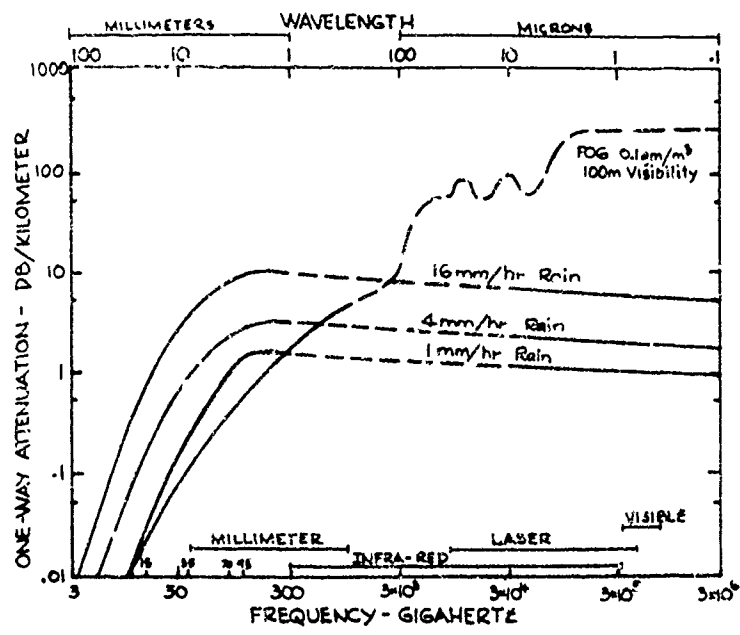
Figure 1. Atmospheric Attenuation as a Function of Frequency

8

TYPE OF CONSTITUENT								
	NATURAL					ACTIVITY RELATED		
Wavelength (Frequency)	Air	Water Vapor	Haze	Fog	Rain	Smoke	Dust	Other
Visual (0.4 - 0.7µ band)	E	G	G	G	A	M	P	P
Near IR - (1.06µ line)	E	A	A	A	A	M	P	P
(1.06µ band)	E	G	A	A	A	M	P	P
Med. IR - (2.3µ band)	E	A	A	A	A	M	P	P
(3.8µ line)	E	A	A	A	A	M	P	P
(3.8µ band)	E	A	A	A	A	M	P	P
Far IR - (10.6µ line)	E	A	A	A	A	M	P	P
(10.6µ band)	E	A	A	A	A	M	P	P
9.375 GHz (X-band)	G	A	A	A	A	M	P	P
35 GHz	G	A	A	A	A	M	P	P
94 GHz	G	A	A	A	A	A	M	P
140 GHz	G	A	A	A	A	A	M	P
240 GHz	G	A	A	A	A	M	P	P

A five letter coding system has been used in this table to evaluate the adequacy of the data base describing the transmission of these constituents. The system is:

E - Excellent - All predictions can be made very accurately.
G - Good   - All predictions can be made to useful accuracy.
A - Adequate - Predictions can sometimes be made to useful accuracy.
M - Marginal - Faulty predictions can result from weak data base.
P - Poor   - Data are too inadequate to make predictions.

The wavelengths addressed in this report were selected for their pertinence to military systems, or potential systems. The microwave frequencies were selected to correspond to those bands having relatively high atmospheric transmission as shown in Figure 1. The visual band was selected for its importance for human target acquisition and because

numerous military systems operate in this region. In the infrared, the
1.06 micron region was selected because of the importance of the neodynium
laser as a designator/illuminator. The 2.3 and 3.8 micron bands were
included because objects of military significance radiate strongly at
these wavelengths. The 3.8 micron laser line (which in reality is
several closely spaced lines) is included because of its potential
application in high-power laser systems. The 10.6 micron region was
selected both because of its nearness to the peak of the radiance
curve for objects at ambient temperature and because of the military
potential of the 10.6 micron carbon dioxide laser. The infrared bands
were also selected because of their high transmission characteristics.
Figure 2, plotted from information contained in Reference 2, shows the
atmospheric transmission as a function of wavelength for 1.0 cm of
water vapor in the line of sight along a 2-km path and clearly shows
the window structure of the infrared absorption spectrum.

This report avoids excessively complicated formulations and,
wherever possible, presents formulas, tables, or graphs which summarize
the available data and gives references where a more comprehensive look
at the physics of the situation can be found. The formulations of
the transmission problem comprise Section II of this report. Finally,
the results will be discussed and exemplified in Section III.

II. ATMOSPHERIC TRANSMISSION

Because of the frequent reference in this report to the atmospheric
attenuation coefficient, it will be described here. It is assumed that
the change in the irradiance (w/cm^2) of radiation traversing an incre-
mental slice dx of a uniform medium is proportional only to the irradiance
(H) in the wavefront and dx. Thus

$$dH = -cHdx \qquad (1)$$

where the minus sign is required since H decreases with distance and
σ is a proportionality constant which is greater than zero. Integrating
equation (1) results in

$$H/H_0 = T = e^{-\sigma x} \qquad (2)$$

where x is now a finite thickness of the medium. H_0, the constant of
integration, is seen to be the initial irradiance, and T is the trans-
mission through a medium of thickness x. The quantity σ is referred
to as the attenuation coefficient for that medium and, in general, is
a function of both the properties of the medium and the wavelength of
the radiation. Equation (2) shows that it has units of inverse length
and that an increase in the attenuation coefficient results in more
rapid attenuation of the radiation.

[2] D.F. Fisher et al, "Transmissometer and Atmospheric-Transmission Studies -
Final Report," University of Michigan, Institute of Science and Technology,
March 1963.

10
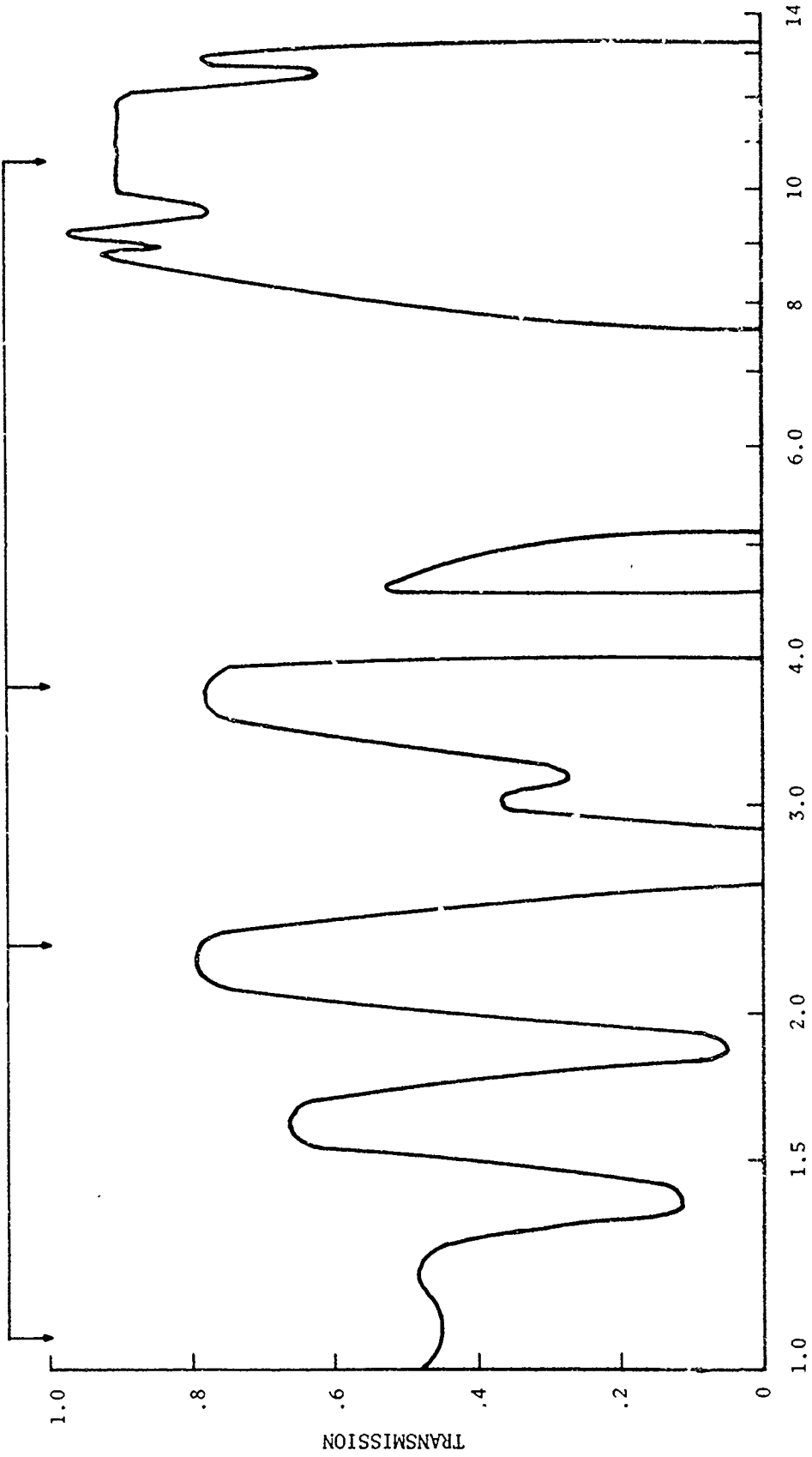
Figure 2. Optical Absorption by Water Vapor

Although in this report procedures will be described whereby transmissions can be predicted, additional information may be needed to address special atmospheres or conditions. For example, if transmissions to high altitudes are of interest, there is a high-altitude ozone band which will strongly attenuate radiation of certain wavelengths. Likewise, if the reader does not wish to go through the procedure of calculating the transmission of each atmospheric constituent and would rather specify some atmospheric characteristics and obtain as an output transmission estimates as a function of wavelength, this report is not likely to be very useful. Those who wish to proceed in this way are advised to take advantage of a large body of research centered at the Air Force Cambridge Research Laboratories. Much information is available from this source in the form of computerized predictions contained in computer code LOWTRAN 3 which is described in Reference 3.

A. Absorption and Scattering by Clear Air

The attenuation by clear air results from two factors, absorption by non-aqueous gases and Rayleigh scattering. Rayleigh scattering is an approximation to the Mie Theory and is descriptive of scattering by particles much smaller than the wavelength of the radiation, i.e., atmospheric gases. The Mie theory, described in Reference 4, is the result of assigning boundary conditions to electromagnetic radiation properties inside and outside a sphere which differs in refractive index from the surrounding medium. The result is a set of differential equations, the solution of which determines the magnitude and direction of the electric and magnetic vectors of the radiation at any point in space. The solution of the equations, however, is tedious even with a digital computer, since it entails summing a pair of very slowly converging infinte series. Some brief results of the Mie Theory will be presented in Section II-C.

An excellent discussion of Rayleigh scattering is given in Reference 5. The Rayleigh scattering mechanism is described by equation (3),

$$\sigma = \frac{32\pi^3}{3N} \frac{(n-1)^2}{\lambda^4} , \qquad (3)$$

[3] J. McClatchey and J. Selby, "Atmospheric Transmittance from 0.25 to 28.5μm: Computer Code LOWTRAN 3," AFCRL-TR-75-0255, May 1975.

[4] G.Mie, "Beitrage zer Optik Truber Medien, Speziell Kolloidales Metallosungen," Ann.der Phys, Vol. 25, 1908.

[5] E.J. McCartney, "Scattering-The Interaction of Light and Matter," Sperry Report No. AB-1272-0057, February 1966.

12

where N is the molecular concentration (2.67×10^{19} cm^{-3} at sea level), n is the index of refraction of pure air, and λ is the wavelength of the radiation. The variable n is only weakly dependent on λ. The following table provides the Rayleigh scattering coefficient as a function of wavelength.

$\lambda(\mu)$	0.55	1.06	2.3	3.8	10.6	1000
$\sigma(\text{km}^{-1})$	1.2×10^{-2}	8.2×10^{-4}	3.7×10^{-5}	5.0×10^{-6}	8×10^{-8}	1×10^{-15}

The value of σ at $\lambda = 0.55\mu$ was obtained by weighting the Rayleigh scattering coefficient throughout the visual spectrum by the response of the human eye. It will be obvious when the values in the table are compared with similar values for other attenuation mechanisms that the last four entries are negligible.

The absorption by non-aqueous gases is negligible in the visual region and, except for a weak carbon dioxide band at 10.6 microns, can also be ignored at the four infrared wavelengths of interest. The transmission of 10.6 micron laser radiation through carbon dioxide is shown in Reference 6 to be characterized by

$$\sigma = 144 \left[\frac{\rho(h)}{\rho(o)}\right]^{15/29} \left(\frac{295}{T}\right)^{3/2} 10^{-970/T} \text{ km}^{-1}, \qquad (4)$$

where $\rho(h)$ is the atmospheric density at an altitude of h kilometres and T is the temperature in degrees Kelvin. This equation is plotted in Figure 3 for ground level conditions.

In the microwave region, the effects of air, water vapor, haze and fog can be combined into a single term which is dependent only on the frequency of the radiation. This continuum attenuation coefficient can be calculated from the solid curve in the bottom graph on Figure 1 by noting that the attenuation in decibels is described by

$$F = -10 \log_{10} T. \qquad (5)$$

Thus an attenuation rate of 1dB/km corresponds to an attenuation coefficient of 0.23 km^{-1}. The values of the attenuation coefficient are therefore

$\nu(\text{GH}_z)$	9.375	35	94	140	240
$\sigma(\text{km}^{-1})$	0	0.016	0.044	0.32	0.14

---

[6]J. Stephenson, W. Haseltine, and C. Moore, Atmospheric Absorption of CO_2 Laser Radiation," Applied Physics Letters, Vol. 11, No. 5, September 1967.
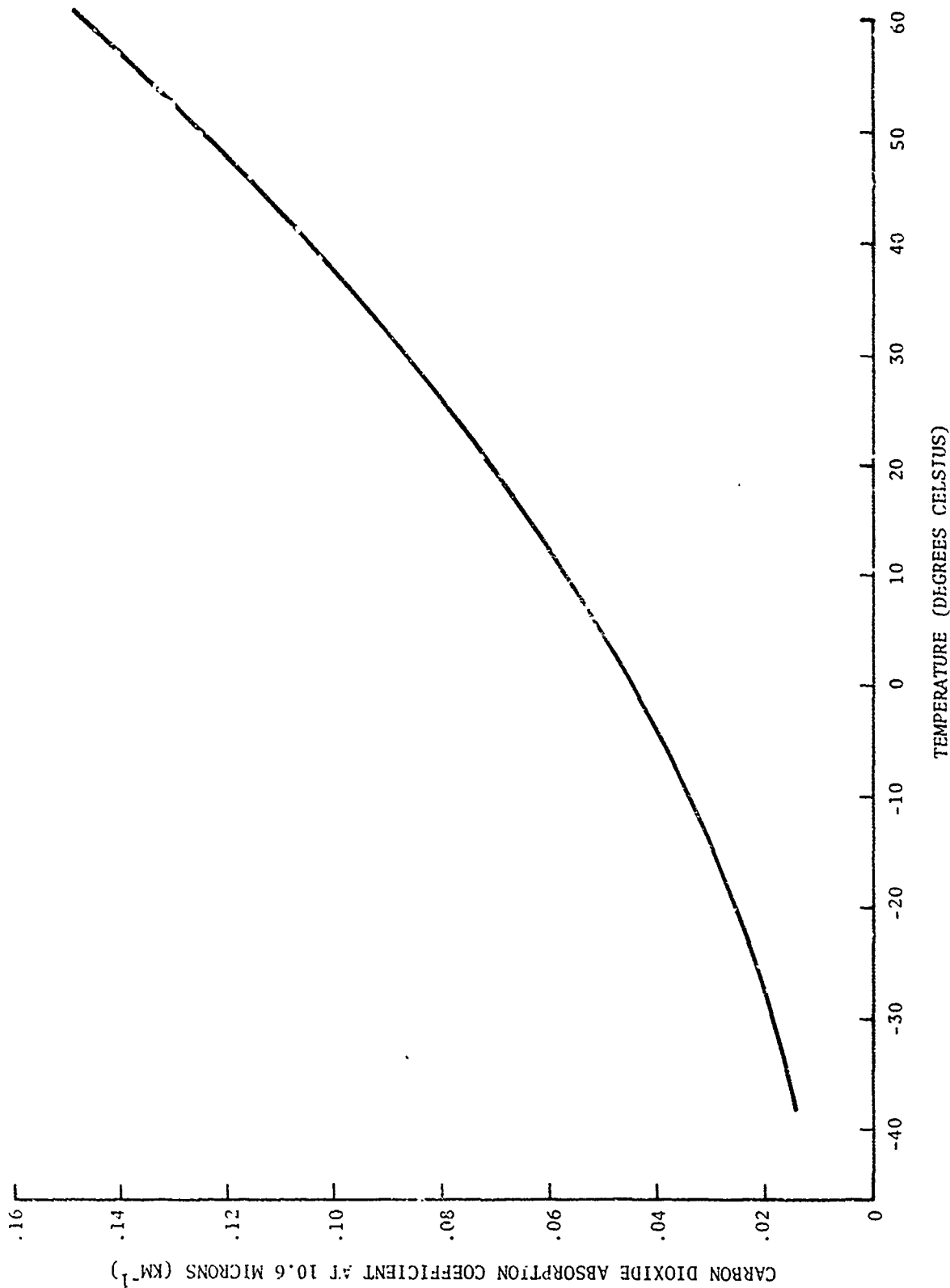
Figure 3. Carbon Dioxide Absorption Coefficient at 10.6 Microns as a Function of Temperature

14

B. Absorption by Water Vapor

Absorption by water vapor in the visual and infrared regions must be addressed separately for the band and line cases. The absorption spectra consist of a large number of narrow and closely spaced absorption bands for which averaging can be performed over wavelength intervals of interest. Since the absorption bands are unresolvable, accurate measurements of absorption of laser radiation should be made using the laser of interest. The broad band case will be discussed first followed by the available information pertinent to laser lines.

A large number of models are available to describe the band attenuation of visible and infrared radiation by water vapor. Three of these models will be described here. The first described by Fisher[2] states that

$$T = A \exp(-CW), \tag{6}$$

where A and C are tabulated in the referenced report as a function of wavelength. W is the number of centimetres of precipitable water vapor in the path which can be calculated from Figure 4. Elder and Strong[7] derived a relationship of the form

$$T = \begin{cases} -k \log_{10} w + t & w \geq w_0 \\ 1.0 & w < w_0 \end{cases} \tag{7}$$

where k, t, and w_0 are empirically determined constants provided for each of nine atmospheric windows (wavelength bands over which the transmission is higher than at adjacent wavelengths). Elsasser[8] developed an error function absorption law of the form

$$T = 1 - \text{erf}(\beta\sqrt{\pi W}/2), \tag{8}$$

where β, the error function absorption coefficient, is tabulated as a function of wavelength.

To illustrate the problems involved in making such calculations, the three models were compared at a wavelength of one micron for which (in equations (6) through (8)) A = 0.48, C = 0, k = 16.5, t = 106.3, and β = 0.10. The results are shown in Figure 5. It is obvious that there

---

[7]T. Elder and J. Strong, "The Infrared Transmission of Atmospheric Windows," J. Franklin Inst., Vol. 255, No. 3, (1953).

[8]W.M. Elsasser, "Heat Transfer by Infrared Radiation in the Atmosphere," Harvard Meteorological Series 6, Harvard University Press, Cambridge, Massachusetts, 1942.
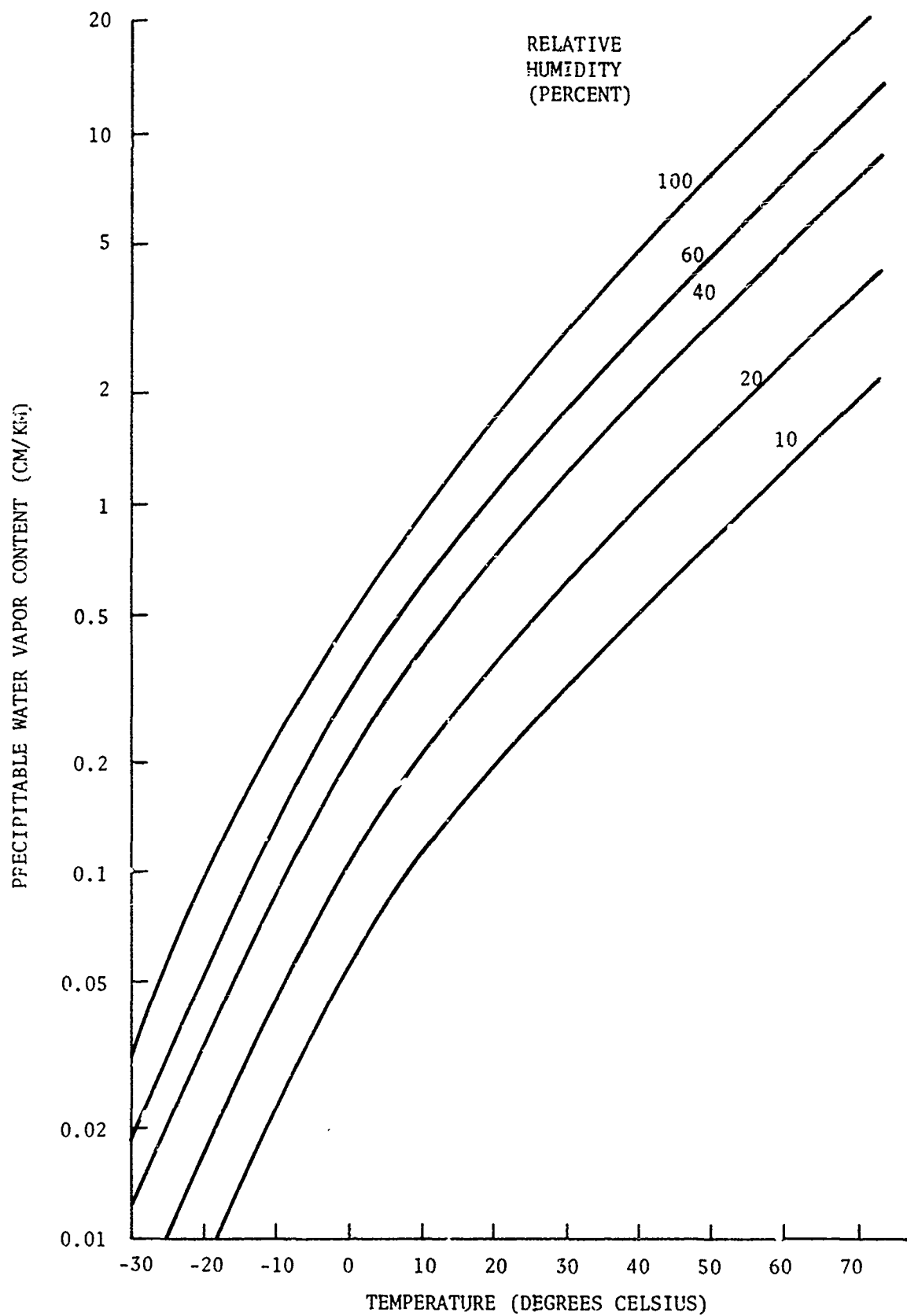
Figure 4. Atmospheric Water Vapor Content

16
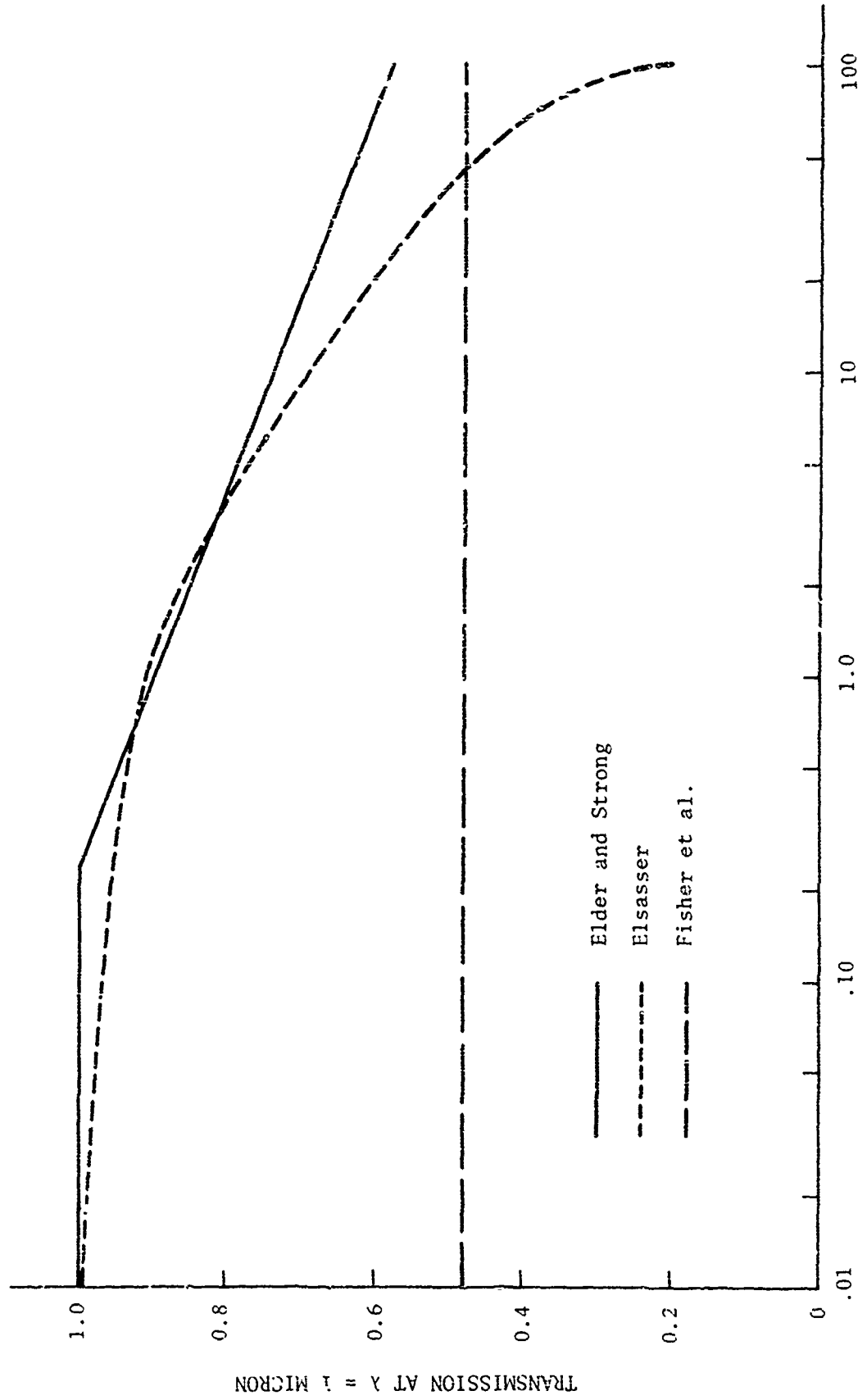
Figure 5. Comparison of Three Water Vapor Absorption Models

Legend (within figure):
Elder and Strong
Elsasser
Fisher et al.

Axis labels:
PRECIPITABLE WATER VAPOR (CM)
TRANSMISSION AT $\lambda = 1$ MICRON

17

is no way that the three models can be reconciled. However, the shape of the Elsasser curve at this wavelength better matches an a priori picture of what the transmission should be. Neither the secondary reference I used to obtain information on the Elsasser model[9] nor the band models of Elder and Strong were able to address long wavelengths, so the model described by Fisher was used for the 10.6 micron situation. The constants used in the models are shown in the following table for which β was weighted by the response curve of the human eye.

$\lambda(\mu)$	Visual	1.06	2.3	3.8	10.6
β	0.118	0.22	0.14	0.55	-
A	-	-	-	-	1.0
C	-	-	-	-	0.0681

Transmission of laser radiation through water vapor follows an exponential absorption law for which an attenuation coefficient can be determined. This is true since the attenuation coefficient for monochromatic radiation is the sum of the contributions from each of the absorption lines, even though the characteristics of the individual lines may not be known. Information on the water vapor absorption of the 1.06 micron laser line was not found, so it will be assumed that it is the same as the band absorption for that wavelength.

Water vapor laser absorption models at 3.8 microns are currently receiving attention from various researchers. A usable model for inclusion in this report was not found, however. Until a satisfactory model is generally available, an assumption that the laser line is attenuated to the same degree as in the described band attenuation will probably suffice since this wavelength is located in a high transmission window.

The absorption of 10.6 micron laser radiation by water vapor has received considerable attention in recent years. As a result, a number of models describing the attenuation mechanism have appeared in the technical literature. An empirical model which seems to work well is described in Reference 10. The model states that

$$\sigma = 4.32 \times 10^{-6} \, p(P + 193p) \; km^{-1}, \tag{9}$$

[9] Henry L. Hackforth, Infrared Radiation, McGraw-Hill Book Company, Inc., 1960,

[10] J. McCoy, D. Rensch, and R. Long, "Water Vapor Continuum Absorption of Carbon Dioxide Laser Radiation Near 10," Applied Optics, Vol. 8, No. 7 1969.

where P is the atmospheric pressure and p is the water vapor partial pressure, both of which are measured in Torr. For standard atmospheric pressure, P is 760. The value of p is a function of temperature and relative humidity and is tabulated in Reference 11. For convenience it is also shown graphically in Figure 6. Equation (9) is plotted for sea level conditions in Figure 7.

C. Scattering by Haze and Fog

As the relative humidity increases in a normal atmosphere, the water vapor will frequently condense about dust or salt nuclei, resulting in an aerosol composed of water droplets. This condition is referred to as haze or fog. The transmission characteristics of haze and fog are generally typified in a rather gross manner by the use of a term called the visibility (V), which is the distance at which a sufficiently large black object situated against the daytime horizon sky can be marginally detected by a human observer. As the number and/ or size of the water droplets is increased the attenuation coefficient increases until at a value of about $\sigma = 4km^{-1}$ (V = 1km), the aerosol loses its selectivity (i.e., the condition wherein radiation of different wavelengths in the visual region is attenuated at different rates). This is the point of transition between haze and fog.[12]

The transmission through both haze and fog can be described by:

$$\sigma = \pi \sum_{r} N_r r^2 K_r, \qquad (10)$$

where the summation is taken over a sufficiently large number of radius bands that droplets of all sizes whose effects are measurable are included. N_r is the number of drops per unit volume with radius r, and K_r is the ratio between the scattering and geometric cross sections and is shown in Figure 8. Since K_r is a slowly varying function of wavelength (based on the index of refraction of water), separate curves are provided for the optical and millimetre wavelengths. Both functions approach two as a limit when r increases rather than one as would be expected. The discrepency is accounted for by diffraction effects.

[11] D.E. Gray, ed, American Institute of Physics Handbook, Second Edition, McGraw-Hill Book Company, Inc., 1963.

[12] W.E.K. Middleton, Vision Through the Atmosphere, University of Toronto Press, Toronto, Canada, 1952.
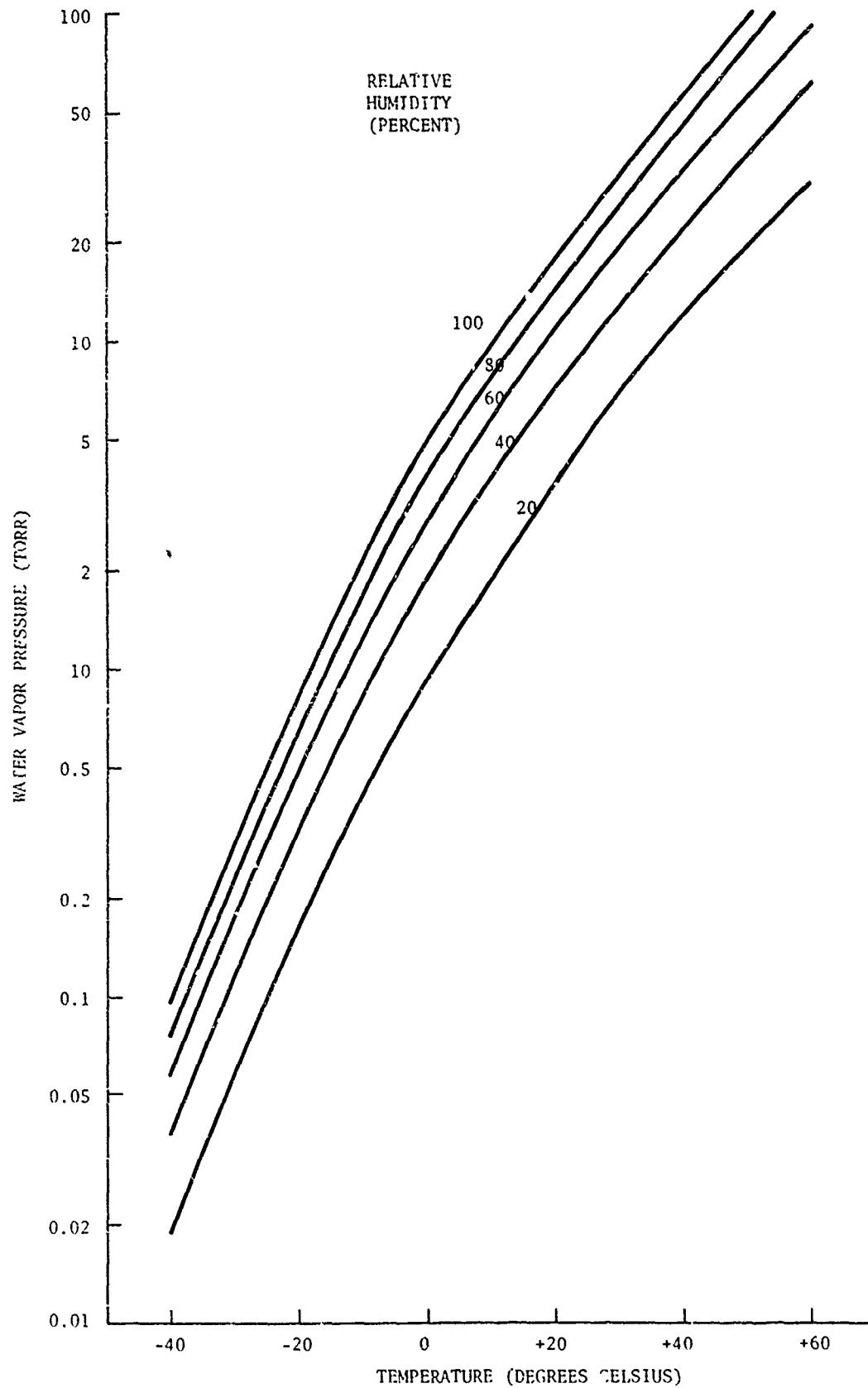
Figure 6. Water Vapor Pressure as a Function of
Temperature and Relative Humidity
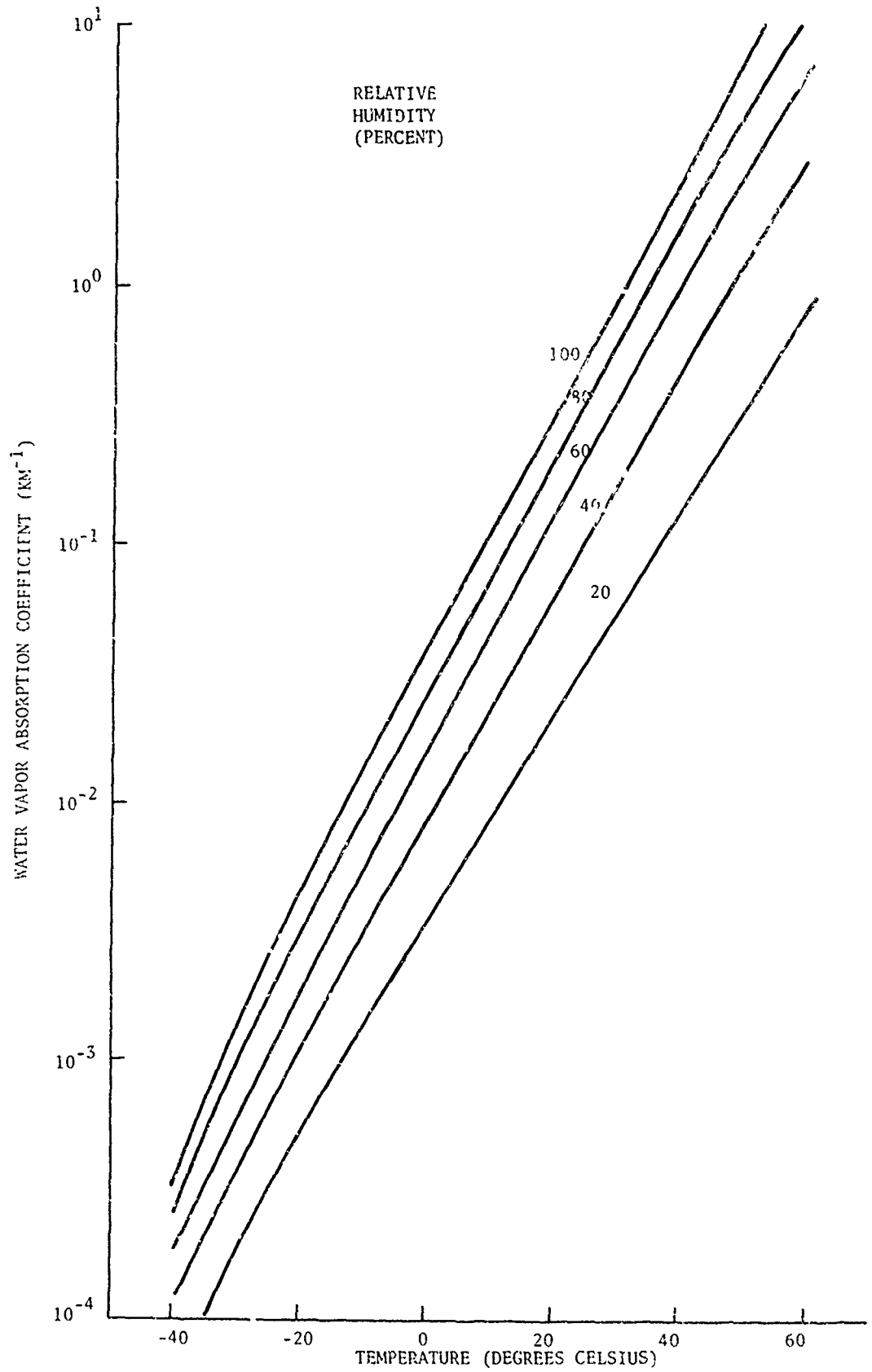
Figure 7. Water Vapor Absorption Coefficient as a Function of Temperature and Relative Humidity

21
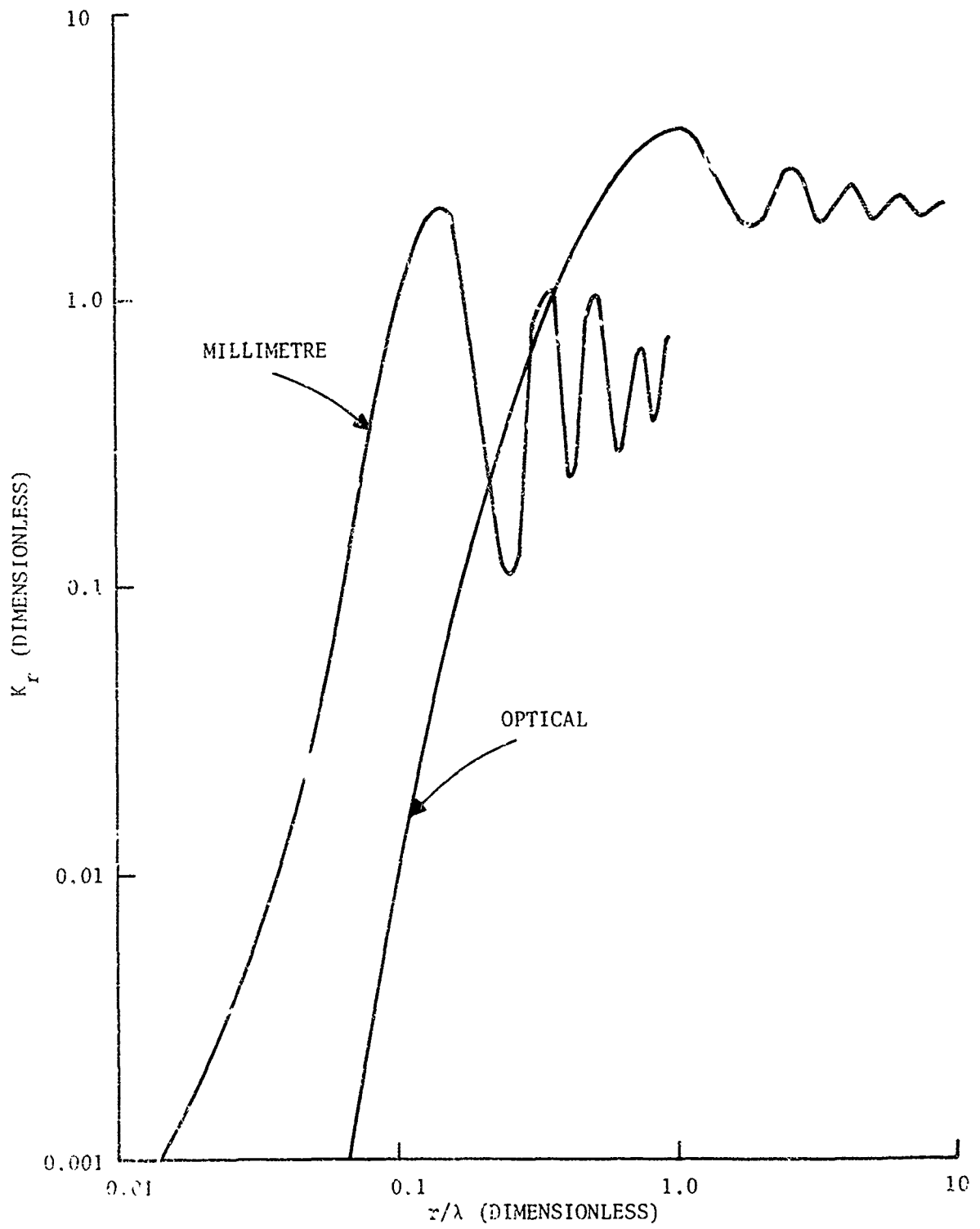
Figure 8 κ_r as a Function of r/λ for the Optical and Millimetre Regions

22

The optical curve was originally generated by Houghton and Chalker.[13] The curve for the millimetre region was plotted from 0.43 cm data in Stephens.[14]

N_r, the droplet radius distribution in a fog, is in large measure characterized by the visibility. The distributions used in this section were taken from Reference 15 and were obtained using a laser fog nephelometer which recorded the drop concentrations in each of 64 radius bands between 2.6 and 242 microns. Eighteen of the radius distributions from Reference 15 were selected for additional analysis. As a first step, the radius bands were revised so that a Δr of one micron could be applied to drops of all sizes. The revised distributions characterized by the visibility extremes in the sample of eighteen are shown in Figure 9. The indicated visibilities are averages of the upper and lower visibility limits reported in Reference 15 which are calculated rather than measured values. Values very close to these were obtained by applying the revised radius distributions of Figure 9 to Equation (10).

A limitation to the data provided in Reference 15 is that no account is taken of droplets with radius less than 2.5 microns. A finding of Dessens[16] indicates that at a relative humidity of 78 percent, the mean droplet radius in a haze is 0.4 microns. In an attempt to include small droplets, the radius bands were again restructured so that the number of drops between r and 1.2r could be specified between r=0.2 and r=70 microns. The curves provided in Reference 15 were then extrapolated subject to a curve maximum of 0.4 micron. This extrapolation process is rather uncertain but was the best procedure among those considered in an attempt to account for the small droplets. The results for the two curves of Figure 9 are shown in Figure 10.

[13] H.G. Houghton and W.R. Chalker, "Scattering Cross Sections of Water Drops in Air for Visible Light," JOSA, Vol. 39, No. 11, November 1949.

[14] J.J. Stephens, "Radar Cross-Sections for Water and Ice Spheres," J. of Meteorology, Vol. 18, 1961.

[15] D.H. Dickson, R.B. Loveland, and W.H. Hatch, "Atmospheric Waterdrop Size Distribution at Capistrano Test Site (CTS) From 16 April Through 11 May 1974 - Vols. IV and V," U.S. Army Atmospheric Sciences Laboratory Report ECOM-DR-75-3, September 1975.

[16] H. Dessens, "Brume et Noyaux de Condensation," Ann de Geophys., Vol. 3, 1947.
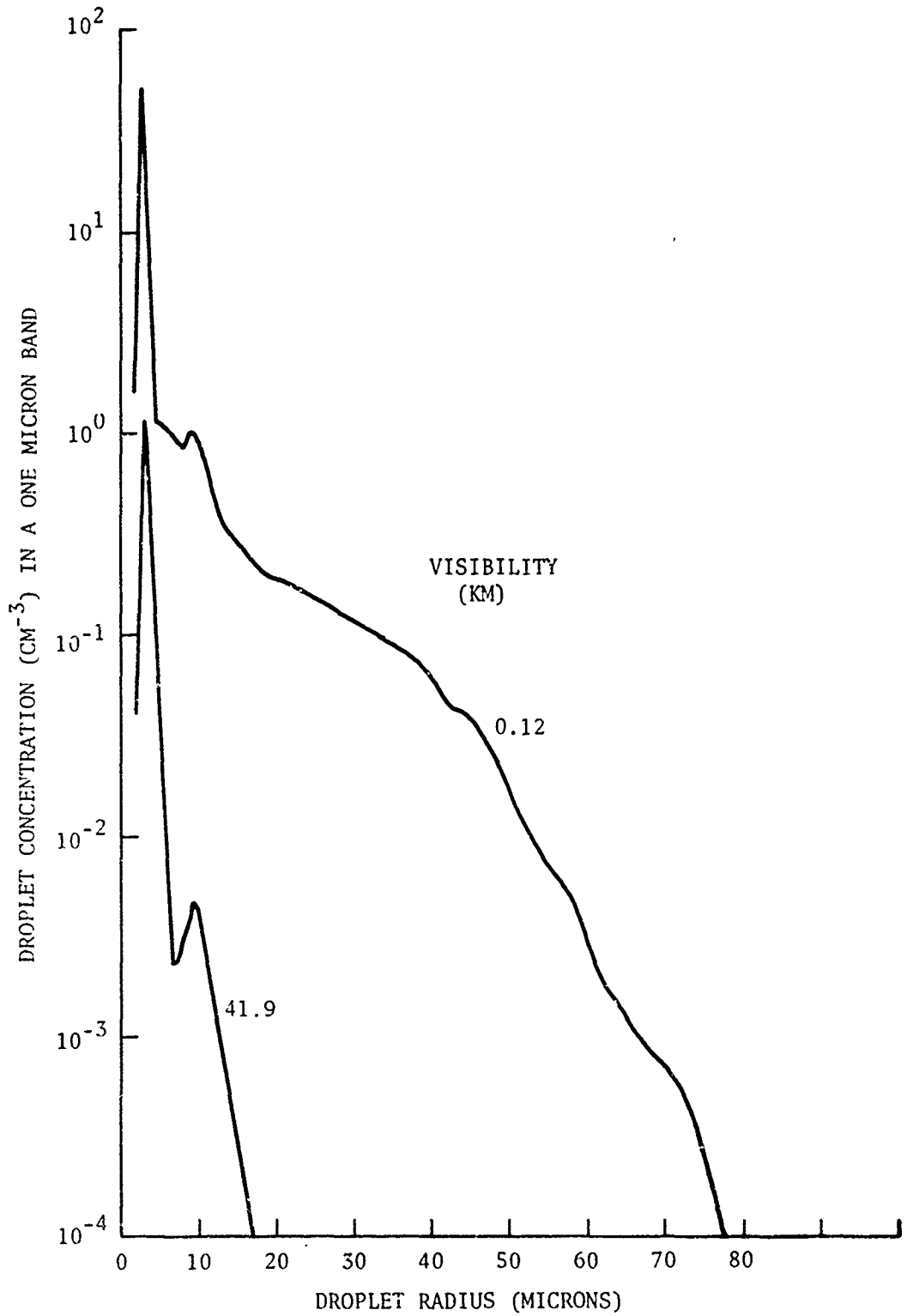
Figure 9.   Droplet Radius Distributions for Two Visibilities
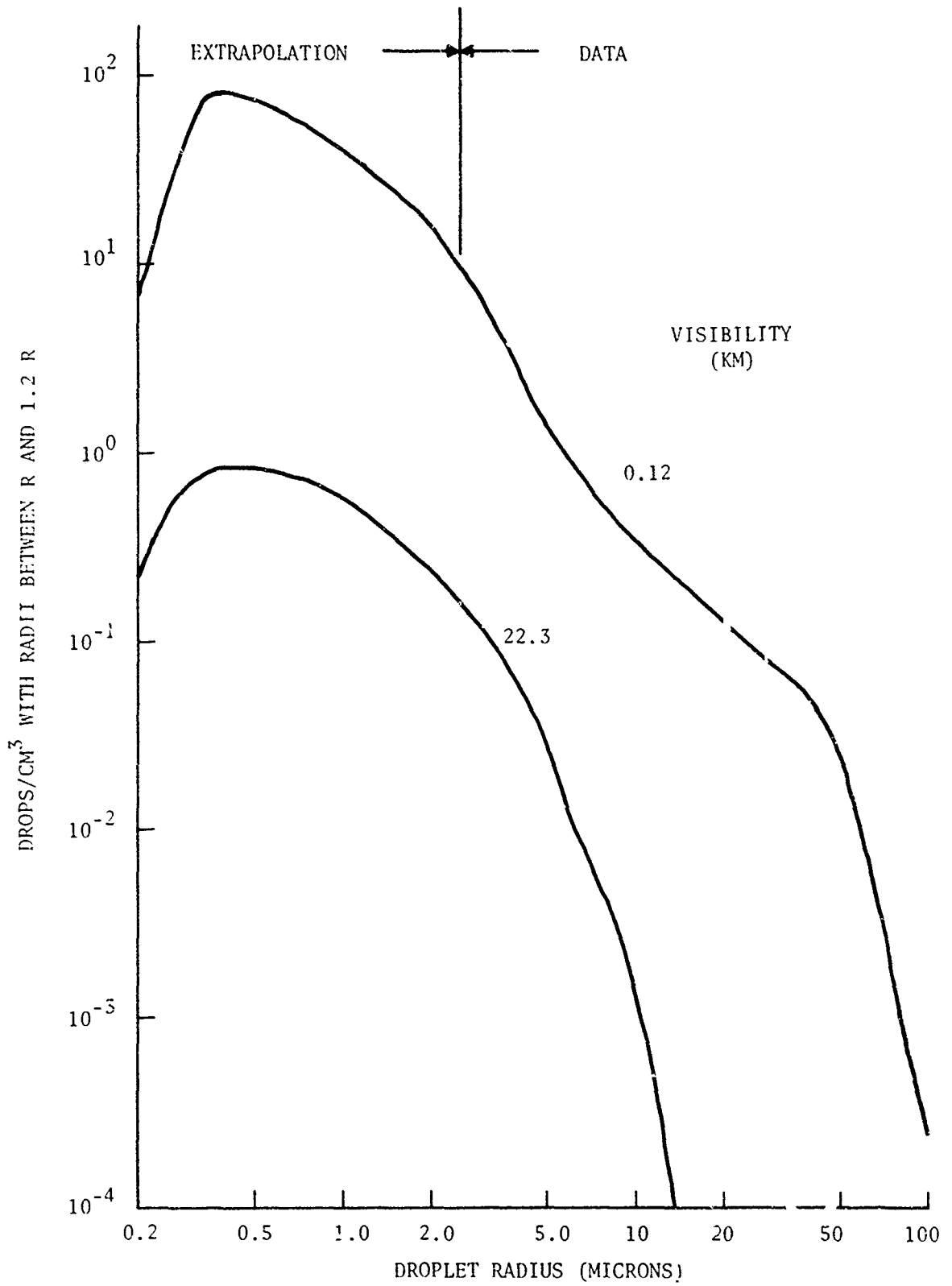
Figure 10. Modified Droplet Radius Distributions for Two Visibilities

It should be noted that the visibility used to characterize the upper curve which was calculated using Equation (10) has dropped from 41.9 to 22.3 km while that of the lower curve has not changed. This phenomenon results from the fact that the addition of small particles will have less effect on a radius distribution containing large numbers of large particles. The reduction in the visibility of the upper curve does not invalidate the visibilities reported in Reference 15 since those visibilities were calculated from the provided data rather than measured independently.

The revised droplet radius distributions of all eighteen samples were then used to calculate the visibility and the corresponding scattering coefficients at the five optical wavelengths. Interpolation of these data resulted in the table below.

VISI-BILITY (KM)	HAZE AND FOG SCATTERING COEFFICIENT (KM^{-1})				
	WAVELENGTH (MICRONS)				
	0.55	1.06	2.3	3.8	10.6
0.1	3.8×10^1	3.8×10^1	3.8×10^1	3.8×10^1	3.8×10^1
0.2	2.2×10^1	2.2×10^1	2.1×10^1	1.9×10^1	1.7×10^1
0.5	9.5×10^0	9.5×10^0	8.7×10^0	6.8×10^0	4.0×10^0
1.0	4.8×10^0	4.8×10^0	4.4×10^0	3.4×10^0	1.0×10^0
2.0	2.2×10^0	2.2×10^0	1.9×10^0	1.5×10^0	2.6×10^{-1}
5.0	9.5×10^{-1}	9.5×10^{-1}	8.5×10^{-1}	6.3×10^{-1}	6.0×10^{-2}
10.0	4.8×10^{-1}	4.8×10^{-1}	4.2×10^{-1}	3.1×10^{-1}	2.7×10^{-2}
20.0	2.4×10^{-1}	2.4×10^{-1}	2.1×10^{-1}	1.5×10^{-1}	1.4×10^{-2}
50.0	9.5×10^{-2}	9.5×10^{-2}	8.3×10^{-2}	5.8×10^{-2}	8.6×10^{-3}

By way of comparison, using the same procedure to determine the scattering coefficient for millimetre radiation yields values between 10^{-4} and 10^{-15}, at least six orders of magnitude below the corresponding optical values. These millimetre wave values are included in the continuum attenuation coefficient discussed earlier.

D.   Scattering by Rain

The transmission through rain in the optical region can be predicted in much the same manner as the transmission through haze and fog by again using Equation (10). It is necessary, however, to select a model describing the appropriate characteristics of the raindrops. A number

26

of empirical models have been developed to describe the radius distribution of raindrops as a function of rainfall rate. References 17 through 20 describe some of the best-known distributions. Here the discussion will be restricted to the drop-size model developed by Best since it seems to fit most accurately the measurements made by BRL personnel with a 70-GHz radar.[21]

The Best model states that for a rainfall rate of R mm/hr, the fraction F(x) of the total liquid water comprised of drops with diameters less than Xmm is

$$F(x) = 1 - \exp\left[-(x/a)^n\right], \tag{11}$$

where

$$a = A \times R^p. \tag{12}$$

The total liquid water content expressed in mm^3/m^3 is

$$W = C \times R^r \tag{13}$$

where $A = 1.30$, $C = 60$, $p = 0.232$, $r = 0.846$, and $n = 2.25$.

These equations were solved for several rainfall rates and the results are shown in Figure 11. The ordinate in this figure is the number of drops per cubic metre with radii between r and 1.2r where r is the drop radius shown on the abscissa. This drop radius distribution was used in Equation (10), resulting in a value of σ for each rainfall rate, wavelength combination. The results are shown in the following table which also includes the visibility.

[17] R.S. Sekhon and R.C. Srivastava, "Doppler Radar Observations of Drop-Size Distribution in a Thunderstorm," J. Atm. Sci., Vol. 28, No. 6, September 1971.

[18] J.S. Marshall and W.M. Palmer, "The Distribution of Raindrops with Size," Journal of Meteorology, Vol. 15, August 1948.

[19] J.O. Laws and D.A. Parsons, "The Relation of Raindrop-Size to Intensity," Transactions, American Geophysical Union, Vol. 24, Part 2, 1943.

[20] A.C. Best, "The Size Distribution of Raindrops," Quarterly Journal Royal Meteorological Society, Vol. 76, 1950.

[21] A.R. Downs, "A Model for Predicting the Rain Backscatter from a 70 GHz Radar," BRL Memo Report No. 2467, March 1975. (AD #A009699)
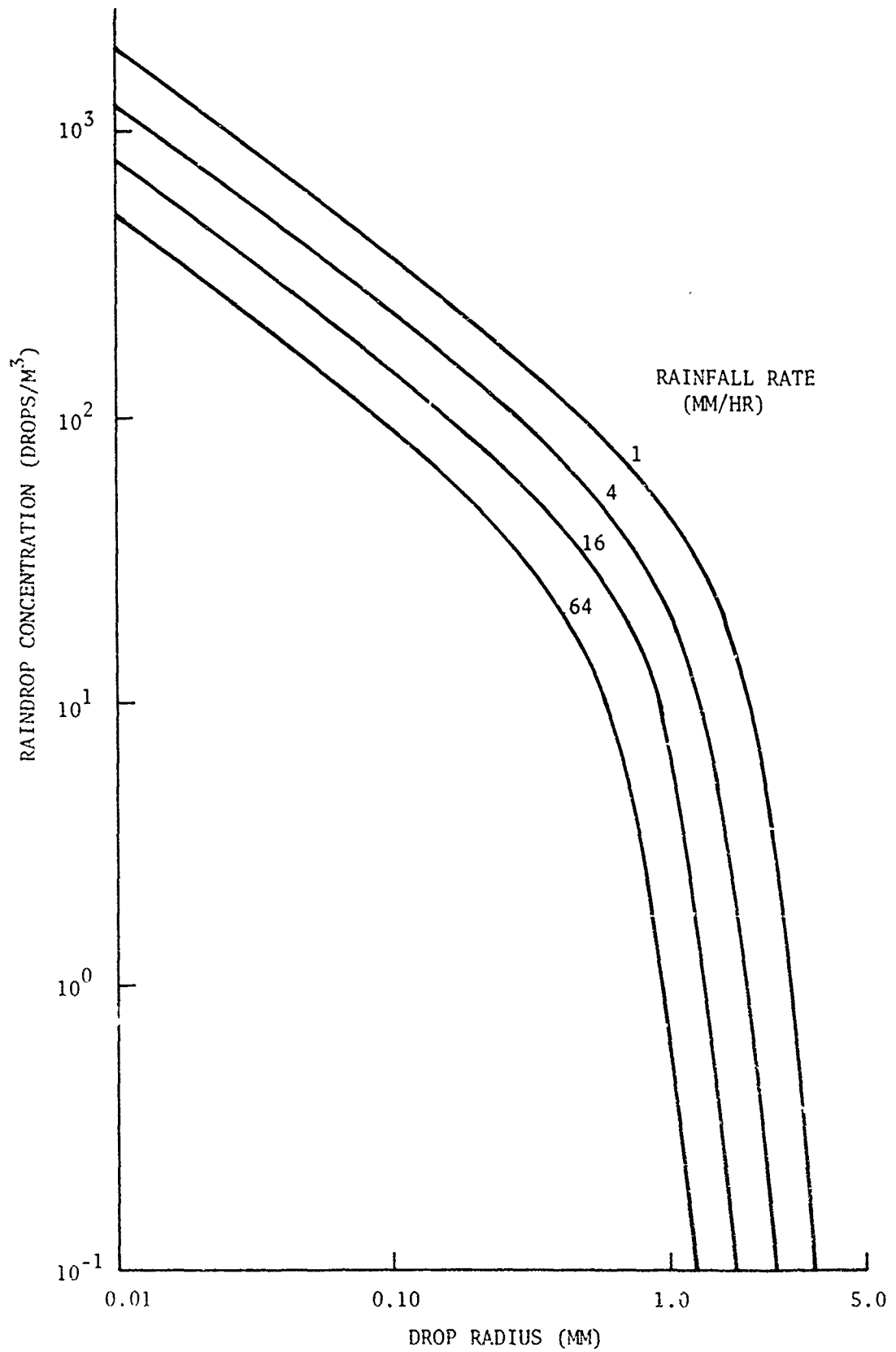
Figure 11   Best Model for Drop Radius Distribution
as a Function of Rainfall Rate

| RAINFALL RATE (MM/HR) | RAIN SCATTERING COEFFICIENT (KM^{-1}) | | | | | VISIBILITY (KM) |
| | WAVELENGTH (MICRONS) | | | | | |
	0.55	1.06	2.3	3.8	10.6	
1	0.245	0.245	0.246	0.246	0.249	16.0
2	0.376	0.376	0.376	0.377	0.381	10.4
4	0.576	0.576	0.576	0.577	0.582	6.8
8	0.882	0.882	0.882	0.883	0.890	4.4
16	1.35	1.35	1.35	1.35	1.36	2.9
32	2.07	2.07	2.07	2.07	2.07	1.9
64	3.17	3.17	3.17	3.17	3.18	1.2

Scattering coefficients in rain at millimetre wavelengths are tabulated in Setzer[22] based on an assumed Laws and Parsons[19] drop radius distribution. Frequencies between 1.43 and 300 GHz and rainfall rates between 0.25 and 150 mm/hr are addressed in this report. Interpolation between the listed values results in the following table.

| RAINFALL RATE (MM/HR) | RAIN SCATTERING COEFFICIENT (KM^{-1}) | | | | |
| | FREQUENCY (GHz) | | | | |
	9.375	35	94	140	240
1	6.0×10^{-5}	1.7×10^{-2}	1.4×10^{-1}	1.6×10^{-1}	1.6×10^{-1}
2	1.7×10^{-4}	4.0×10^{-2}	2.3×10^{-1}	2.4×10^{-1}	2.4×10^{-1}
4	4.7×10^{-4}	8.5×10^{-2}	3.7×10^{-1}	3.8×10^{-1}	3.8×10^{-1}
8	1.4×10^{-3}	1.8×10^{-1}	6.4×10^{-1}	6.4×10^{-1}	6.4×10^{-1}
16	4.0×10^{-3}	4.0×10^{-1}	1.1×10^{0}	1.1×10^{0}	1.1×10^{0}
32	1.2×10^{-2}	8.2×10^{-1}	1.8×10^{0}	1.8×10^{0}	1.8×10^{0}
64	3.2×10^{-2}	1.7×10^{0}	2.9×10^{0}	2.9×10^{0}	2.9×10^{0}

[22] D.E. Setzer, "Computed Transmission Through Rain at Microwave and Visible Frequencies," BSTJ, Vol. 49, 1970.

E. Absorption by Water Drops

A useful procedure for calculating the relative effects of optical absorption and scattering from water drops is provided by Zanotelli[23] and is summarized in Middleton.[12] Although somewhat limited in its applicability, the technique will be briefly summarized based on Middleton's discussion. It should first be noted that the approach is useful only under those conditions which permit the approximation

$$1 - \exp\,(-2\sigma r) = 2\sigma r, \tag{14}$$

where σ is the absorption coefficient for liquid water and r is the drop radius. It will be assumed that an error of 20 percent is allowable, resulting in the useful limit that $\sigma r < 0.232$. The relative energy removed from the wavefront through absorption by a drop of radius r is

$$U_A = \frac{4}{3}\,\pi r^3 (\sigma/\mu), \tag{15}$$

where μ is the index of refraction of water. The corresponding value for scattering is

$$U_S = \pi r^2 K_r. \tag{16}$$

The relative effectiveness of absorption vis-a-vis scattering is the ratio between the two expressions, namely

$$U_A/U_S = \frac{4r}{3K_r}\,(\frac{\sigma}{\mu}). \tag{17}$$

The mean drop radius in haze, fog, and rain can be calculated from the radius distributions discussed previously and K_r is given by Figure 8. Values for σ and μ can be found in both Middleton[12] and Deirmendjian[24], although they are not listed for exactly the values addressed in this report. Also, the wide variations found in σ make interpolation impossible, so those wavelengths closest to those addressed in this report will be utilized. The following table summarizes the available information.

[23]G. Zanotelli, "Assorbimento Elementare Della Luce nel Passagio Attraverso Alle Nubi," Atti. Accad. Ital., Rend. Cl. Sci. Fis. Mat. Nat., Vol. 2, 1940.

[24]D. Deirmendjian, Electromagnetic Scattering on Spherical Polydispersions, American Elsevier Publishing Company, Inc., New York, 1969.

WAVELENGTH (MICRONS)	σ (CM^{-1})	μ	DROP TYPE	QUANTIFIER	r (CM)	$r\sigma$	APPROX. VALID?	K_r	u_A/u_S
0.55	2×10^{-2}	1.33	Haze	V = 50 km	.000091	1.8×10^{-6}	Yes	2.0	5.6×10^{-7}
				20	.000095	1.9×10^{-6}			5.8×10^{-7}
				10	.000097	1.9×10^{-6}			5.9×10^{-7}
				5	.000100	2.0×10^{-6}			6.2×10^{-7}
				2	.000103	2.0×10^{-6}			6.3×10^{-7}
				1	.000106	2.1×10^{-6}			6.5×10^{-7}
			Fog	.5	.000108	2.1×10^{-6}			6.6×10^{-7}
				.2	.000112	2.2×10^{-6}			6.8×10^{-7}
				.1	.000116	2.3×10^{-6}			7.1×10^{-7}
			Rain	R = 1 mm/hr	.054	1.1×10^{-3}			3.4×10^{-4}
				2	.060	1.2×10^{-3}			3.7×10^{-4}
				4	.067	1.3×10^{-3}			4.0×10^{-4}
				8	.080	1.6×10^{-3}			5.0×10^{-4}
				16	.096	1.9×10^{-3}			5.9×10^{-4}
				32	.110	2.2×10^{-3}			6.8×10^{-4}
				64	.130	2.6×10^{-3}			8.1×10^{-4}

WAVELENGTH (MICRONS)	σ (CM^{-1})	μ	DROP TYPE	QUANTI-FIER	r (CM)	rσ	APPROX.	K_r	U_A/U_S
1.19	1.056	1.322	Haze	V = 50 km	.000091	9.6×10^{-5}	Yes	3.1	3.2×10^{-5}
				20	.000095	1.0×10^{-4}		3.2	3.2×10^{-5}
				10	.000097	1.0×10^{-4}		3.2	3.2×10^{-5}
			Fog	5	.000100	1.1×10^{-4}		3.3	3.3×10^{-5}
				2	.000103	1.1×10^{-4}		3.4	3.3×10^{-5}
				1	.000106	1.1×10^{-4}		3.5	3.2×10^{-5}
				.5	.000108	1.1×10^{-4}		3.6	3.1×10^{-5}
				.2	.000112	1.2×10^{-4}		3.7	3.2×10^{-5}
				.1	.000114	1.2×10^{-4}		3.8	3.2×10^{-5}
			Rain	R = 1 mm/hr	.054	5.7×10^{-2}		2.0	2.9×10^{-2}
				2	.060	6.3×10^{-2}			3.2×10^{-2}
				4	.067	7.1×10^{-2}			3.6×10^{-2}
				8	.080	8.4×10^{-2}			4.2×10^{-2}
				16	.096	1.0×10^{-1}			5.0×10^{-2}
				32	.110	1.2×10^{-1}			6.1×10^{-2}
				64	.130	1.4×10^{-1}			7.1×10^{-2}

WAVELENGTH (MICRONS)	σ (CM^{-1})	μ	DROP TYPE	QUANTI-FIER	r (CM)	$r\sigma$	APPROX. VALID?	K_r	U_A/U_S
2.25	19.55	1.29	Haze	V = 50 km	.000091	1.8×10^{-3}	Yes	1.2	1.6×10^{-3}
				20	.000095	1.9×10^{-3}		1.3	1.5×10^{-3}
				10	.000097	1.9×10^{-3}		1.4	1.4×10^{-3}
				5	.000100	2.0×10^{-3}		1.5	1.4×10^{-3}
				2	.000103	2.0×10^{-3}		1.6	1.3×10^{-3}
				1	.000106	2.1×10^{-3}		1.8	1.2×10^{-3}
			Fog	.5	.000108	2.1×10^{-3}		1.9	1.1×10^{-3}
				.2	.000112	2.2×10^{-3}	No	2.0	1.1×10^{-3}
				.1	.000114	2.2×10^{-3}		2.0	1.1×10^{-3}
			Rain	R = 1 mm/hr	.054	1.1×10^{0}		2.0	2.3×10^{-1}
				2	.060	1.2×10^{0}			2.3×10^{-1}
				4	.067	1.3×10^{0}			2.4×10^{-1}
				8	.080	1.6×10^{0}			2.5×10^{-1}
				16	.096	1.9×10^{0}			2.5×10^{-1}
				32	.110	2.2×10^{0}			2.6×10^{-1}
				64	.130	2.5×10^{0}			2.6×10^{-1}

33

WAVELENGTH (MICRONS)	σ (CM^{-1})	μ	DROP TYPE	QUANTI-FIER	r (CM)	$r\sigma$	APPROX. VALID?	K_r	U_A/U_S
3.90	190.1	1.353	Haze	V = 50 km	.000091	1.7×10^{-2}	Yes	0.29	5.8×10^{-2}
				20	.000095	1.8×10^{-2}		0.31	5.6×10^{-2}
				10	.000097	1.8×10^{-2}		0.35	5.1×10^{-2}
				5	.000100	1.9×10^{-2}		0.39	4.8×10^{-2}
				2	.000103	2.0×10^{-2}		0.45	4.4×10^{-2}
			Fog	1	.000106	2.0×10^{-2}		0.48	4.2×10^{-2}
				.5	.000108	2.1×10^{-2}		0.51	4.1×10^{-2}
				.2	.000112	2.1×10^{-2}		0.54	4.0×10^{-2}
				.1	.000114	2.2×10^{-2}		0.56	3.9×10^{-2}
			Rain	R = 1 mm/hr	.054	1.0×10^{1}	No	2.0	2.5×10^{-1}
				2	.060	1.1×10^{1}			2.5×10^{-1}
				4	.067	1.3×10^{1}			2.5×10^{-1}
				8	.080	1.5×10^{1}			2.5×10^{-1}
				16	.096	1.8×10^{1}			2.5×10^{-1}
				32	.110	2.1×10^{1}			2.5×10^{-1}
				64	.130	2.5×10^{1}			2.5×10^{-1}

WAVELENGTH (MICRONS)	σ (CM^{-1})	μ	DROP TYPE	QUANTIFIER	r (CM)	$r\sigma$	APPROX. VALID?	K_r	η_A/η_S
10.0	755.2	1.212	Haze	V = 50 km	.000091	.069	Yes	.0056	6.8×10^0
				20	.000095	.072		.0070	5.7×10^0
				10	.000097	.073		.0080	5.0×10^0
				5	.000100	.076		.0100	4.2×10^0
				2	.000103	.078		.0112	3.8×10^0
				1	.000106	.080		.0128	3.4×10^0
			Fog	.5	.000108	.082		.0140	3.2×10^0
				.2	.000112	.085		.0165	2.8×10^0
				.1	.000114	.086		.0190	2.5×10^0
			Rain	R = 1 mm/hr	.054	4.1×10^1	No	2.0	2.8×10^{-1}
				2	.060	4.5×10^1			2.8×10^{-1}
				4	.067	5.1×10^1			2.8×10^{-1}
				8	.080	6.0×10^1			2.8×10^{-1}
				16	.096	7.2×10^1			2.8×10^{-1}
				32	.110	8.3×10^1			2.8×10^{-1}
				64	.130	9.8×10^1			2.8×10^{-1}

In those cases where the Zanotelli approximation is not valid, the absorption-to-scattering ratio was calculated from the equation

$$U_A/U_S = \frac{2}{3 \mu K_r} (1 - e^{-2r\sigma}).$$ (18)

The values in the preceding table were applied to the scattering coefficients shown earlier. The results are shown in the next two tables.

VISI-BILITY (KM^{-1})	HAZE AND FOG ABSORPTION COEFFICIENT (KM^{-1})				
	WAVELENGTH (MICRONS)				
	0.55	1.06	2.3	3.8	10.6
0.1	2.7×10^{-5}	1.2×10^{-3}	3.2×10^{-2}	1.5×10^{0}	9.5×10^{1}
0.2	1.5×10^{-5}	7.0×10^{-4}	2.3×10^{-2}	7.6×10^{-1}	4.8×10^{1}
0.5	6.3×10^{-6}	2.9×10^{-4}	9.6×10^{-3}	2.8×10^{-1}	1.3×10^{1}
1.0	3.1×10^{-6}	1.5×10^{-4}	5.3×10^{-3}	1.4×10^{-1}	3.4×10^{0}
2.0	1.4×10^{-6}	7.3×10^{-5}	2.5×10^{-3}	6.6×10^{-2}	9.0×10^{-1}
5.0	5.9×10^{-7}	3.1×10^{-5}	1.2×10^{-3}	3.0×10^{-2}	2.5×10^{-1}
10.0	2.8×10^{-7}	1.5×10^{-5}	5.9×10^{-4}	1.6×10^{-2}	1.4×10^{-1}
20.0	1.4×10^{-7}	7.7×10^{-6}	3.2×10^{-4}	3.4×10^{-3}	8.0×10^{-2}
50.0	5.3×10^{-8}	3.0×10^{-6}	1.3×10^{-4}	3.4×10^{-3}	5.8×10^{-2}

RAINFALL RATE (MM/HR)	RAIN ABSORPTION COEFFICIENT (KM^{-1})				
	WAVELENGTH (MICRONS)				
	0.55	1.06	2.3	3.8	10.6
1	8.3×10^{-5}	7.1×10^{-3}	5.7×10^{-2}	6.2×10^{-2}	7.0×10^{-2}
2	1.4×10^{-4}	1.2×10^{-2}	8.6×10^{-2}	9.4×10^{-2}	1.0×10^{-1}
4	2.3×10^{-4}	2.1×10^{-2}	1.2×10^{-1}	1.4×10^{-1}	1.6×10^{-1}
8	4.4×10^{-4}	3.7×10^{-2}	2.2×10^{-1}	2.2×10^{-1}	2.5×10^{-1}
16	8.0×10^{-4}	6.8×10^{-2}	3.4×10^{-1}	3.4×10^{-1}	3.8×10^{-1}
32	1.4×10^{-3}	1.3×10^{-1}	5.4×10^{-1}	5.2×10^{-1}	5.8×10^{-1}
64	2.6×10^{-3}	2.3×10^{-1}	8.2×10^{-1}	7.9×10^{-1}	8.9×10^{-1}

Absorption coefficients in rain are provided in Setzer[22] as a function of rainfall rate and frequency, again based on the Laws and Parsons[19] drop radius distribution. Interpolation between the values provided in this reference results in the following table.

RAINFALL RATE (MM/HR)	RAIN ABSORPTION COEFFICIENT (KM^{-1})				
	FREQUENCY (GHz)				
	9.375	35	94	140	240
1	2.0×10^{-3}	4.6×10^{-2}	1.2×10^{-1}	1.4×10^{-1}	1.4×10^{-1}
2	4.8×10^{-3}	8.7×10^{-2}	2.0×10^{-1}	2.3×10^{-1}	2.3×10^{-1}
4	1.2×10^{-2}	1.6×10^{-1}	3.3×10^{-1}	3.7×10^{-1}	3.7×10^{-1}
8	2.9×10^{-2}	3.0×10^{-1}	5.4×10^{-1}	6.2×10^{-1}	6.2×10^{-1}
16	6.5×10^{-2}	5.6×10^{-1}	8.7×10^{-1}	1.0×10^{0}	1.0×10^{0}
32	1.6×10^{-1}	1.0×10^{0}	1.5×10^{0}	1.7×10^{0}	1.7×10^{0}
64	3.8×10^{-1}	1.8×10^{0}	2.3×10^{0}	2.6×10^{0}	2.6×10^{0}

F. Attenuation by Smoke and Dust

Transmission of optical radiation through smoke, dust, and other battlefield contaminants is less adequately documented than is the case with natural constituents. Some data are available on smoke transmission, but the level of predictability is low in any solution of practical problems. Compared to the naturally occurring constituents, the positional and temporal character of the obscuring smokes and their dependence on humidity and wind properties are less accurately known. The available smoke data are generally of two kinds. The first kind is exemplified by Figure 12, taken from Allen and Simonson.[25] Note that the data are expressed in terms of attenuation rather than the transmission which is more common. The transmissions are over a path length of ten metres. Information like this is generally very difficult to apply since the concentration on a battlefield will vary drastically in both time and place in manners which cannot now be predicted with any reliability.

---

[25] G. Allen and B. Simonson, "Attenuation of Infrared Laser Radiation by HC, FS, WP, and Fog Oil Smokes," Edgewood Arsenal Technical Report EATR 4405, May 1970.
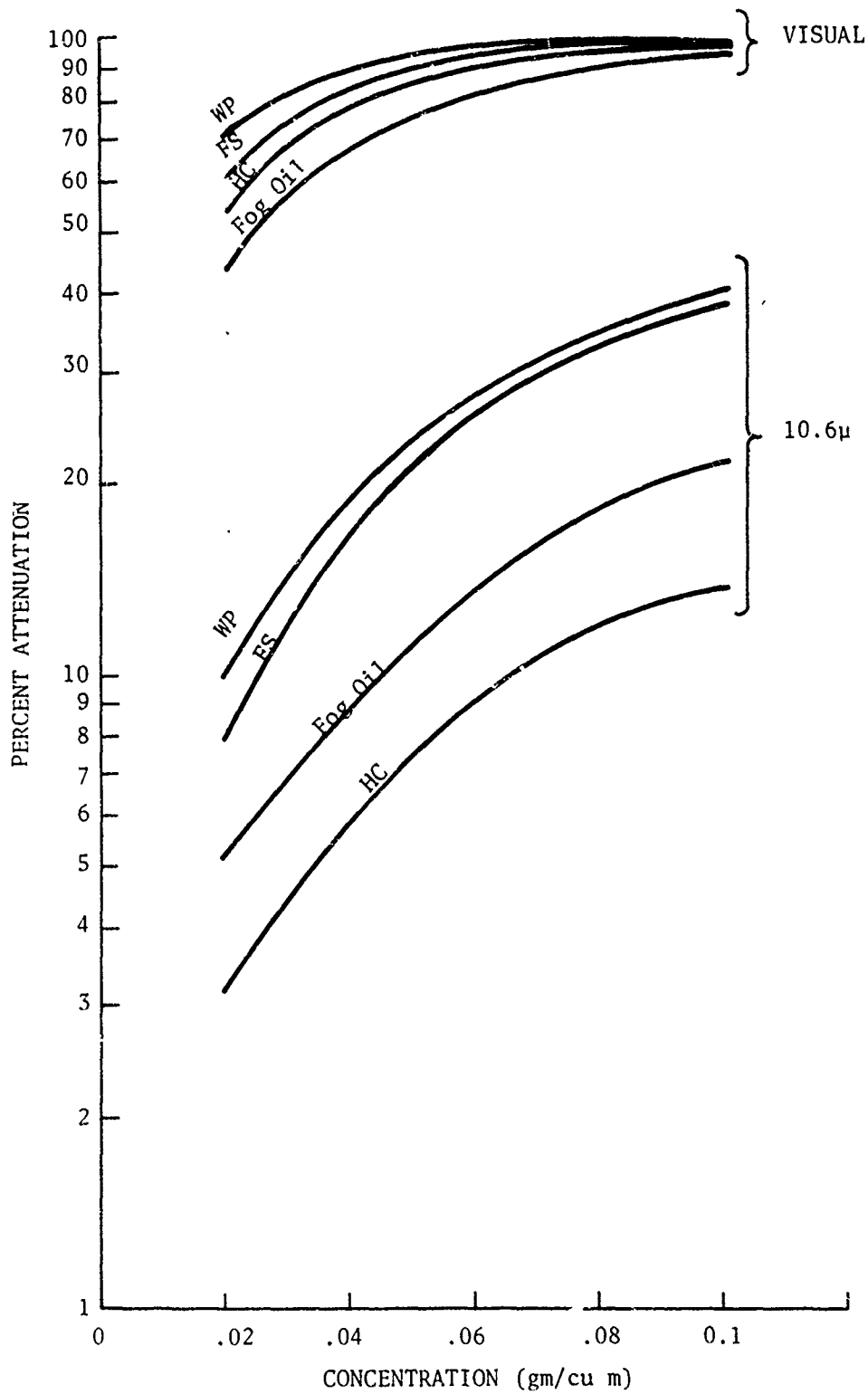
Figure 12. Transmission through Several Smokes as a
Function of Concentration

38

The other kind of attenuation information results from measurements made in the field. Three recent smoke attenuation measurement programs in which BRL personnel have participated have resulted in a substantial data base on smoke attenuation in battlefield environments. These programs were conducted at Fort Sill, Oklahoma, in December 1975, at Fort Hood, Texas, in March 1976, and at Aberdeen Proving Ground (APG), Maryland, in June 1976. At Fort Sill, HC and WP smoke was delivered by live firings of mortar and artillery weapons. At Fort Hood, smoke was provided by 2.75-inch WP wick rounds. At APG, smoke was generated by HC and fog oil pots and statically detonated 155mm WP rounds. In each test, broad-band attenuation measurements were made in the visual, 0.7-1.1 micron, 3-5 micron, and 8-14 micron regions. In addition, the APG tests included measurements using 94- and 140-GHz radars.

The data collected in these tests are extensive, and a large sample will be published in the near future.[26] In this report, several examples will be provided which are typical of the data collected. Figures 13 through 15 show the transmission as a function of time for several different smokes. Figure 13 represents the transmission through the cloud produced by a 105mm HC round. Figure 14 shows the effects of a 60mm mortar WP round. Both sets of measurements were made at Fort Sill. On both, there was no measurable difference between the 3-5 and 8-14 micron bands, so they are shown as one curve. The much more rapid dissipation rate of the WP smoke is caused by the mushrooming effect due to the highly exothermic nature of the reaction causing the smoke. Figure 15 shows the transmission through the cloud produced by nine M7 fog oil smoke pots used in the APG tests. In this case, the visual and the 0.7-1.1 micron transmissions were almost identical. The 94- and 140-GHz radars were operated during this test, and the resulting signals showed no attenuation.

Data of the form shown by Figures 13-15 are useful in that they document a real situation which could occur in a combat environment, and are therefore more believable than measurements made in the laboratory. The drawbacks of this approach are that the fine characteristics of the curves cannot be predicted in advance and there is no way to predict how the curves would change if there was a change in release point , delivery technique, wind velocity or direction, temperature, pressure, relative humidity, ground condition, height of measurement, wavelength, type of agent, etc. A summary of some pertinent results from all three test series is shown in the following table in which the times are all expressed in minutes.

---

[26]R.G. Reitz. 'An Analysis of Smoke Transmission Measurements and Techniques," BRL Memorandum Report (in preparation).

Figure 13. Optical Transmission Through an HC Smoke Cloud

WAVELENGTH
(MICRONS)

3-5 and 8-14

0.7-1.1

0.4-0.7

TRANSMISSION

1.0

0.8

0.6

0.4

0.2

0

0

20

40

60

80

100

120

140

TIME AFTER IMPACT (SECONDS)

40
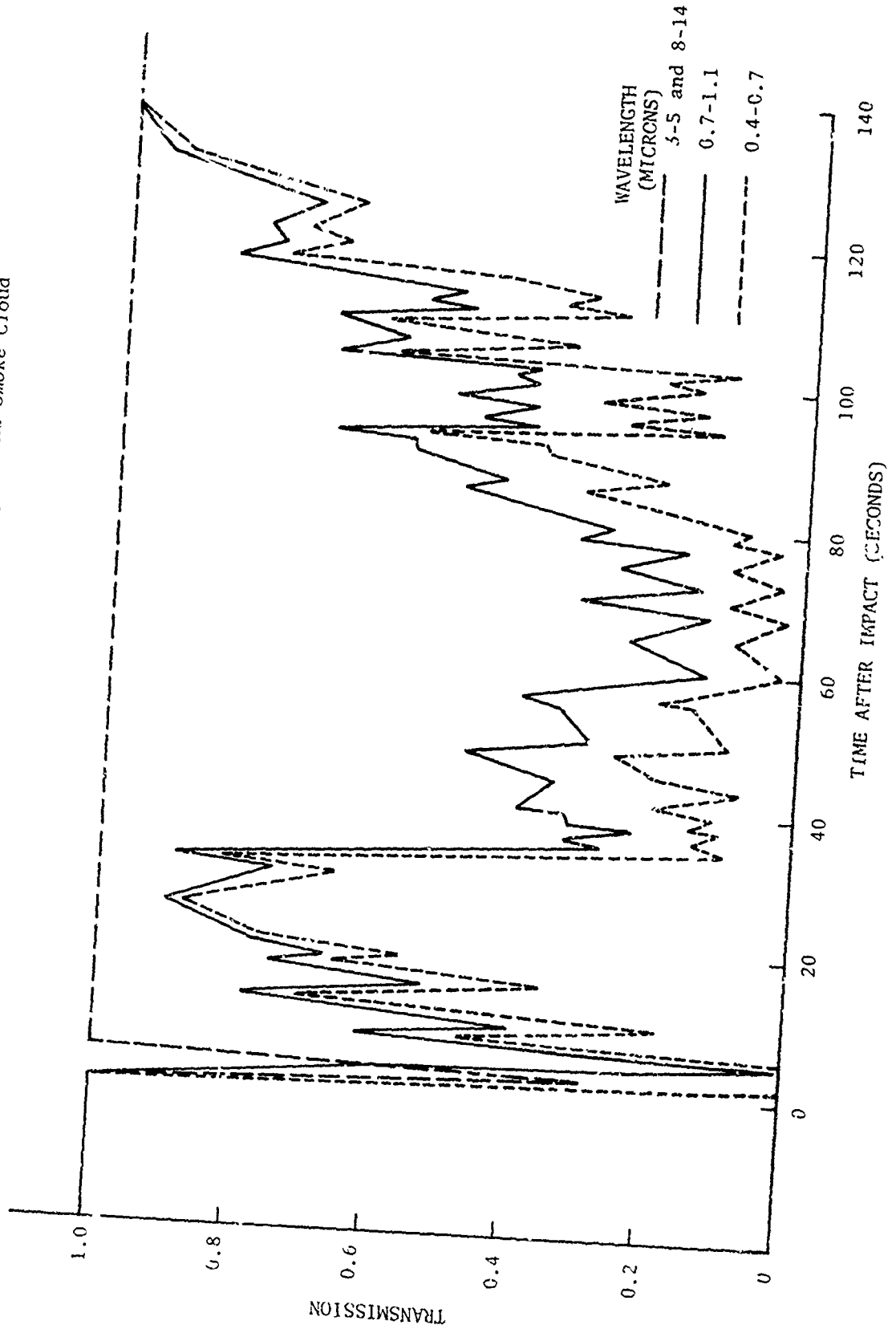
Figure 14. Optical Transmission Through a WP Smoke Cloud

41
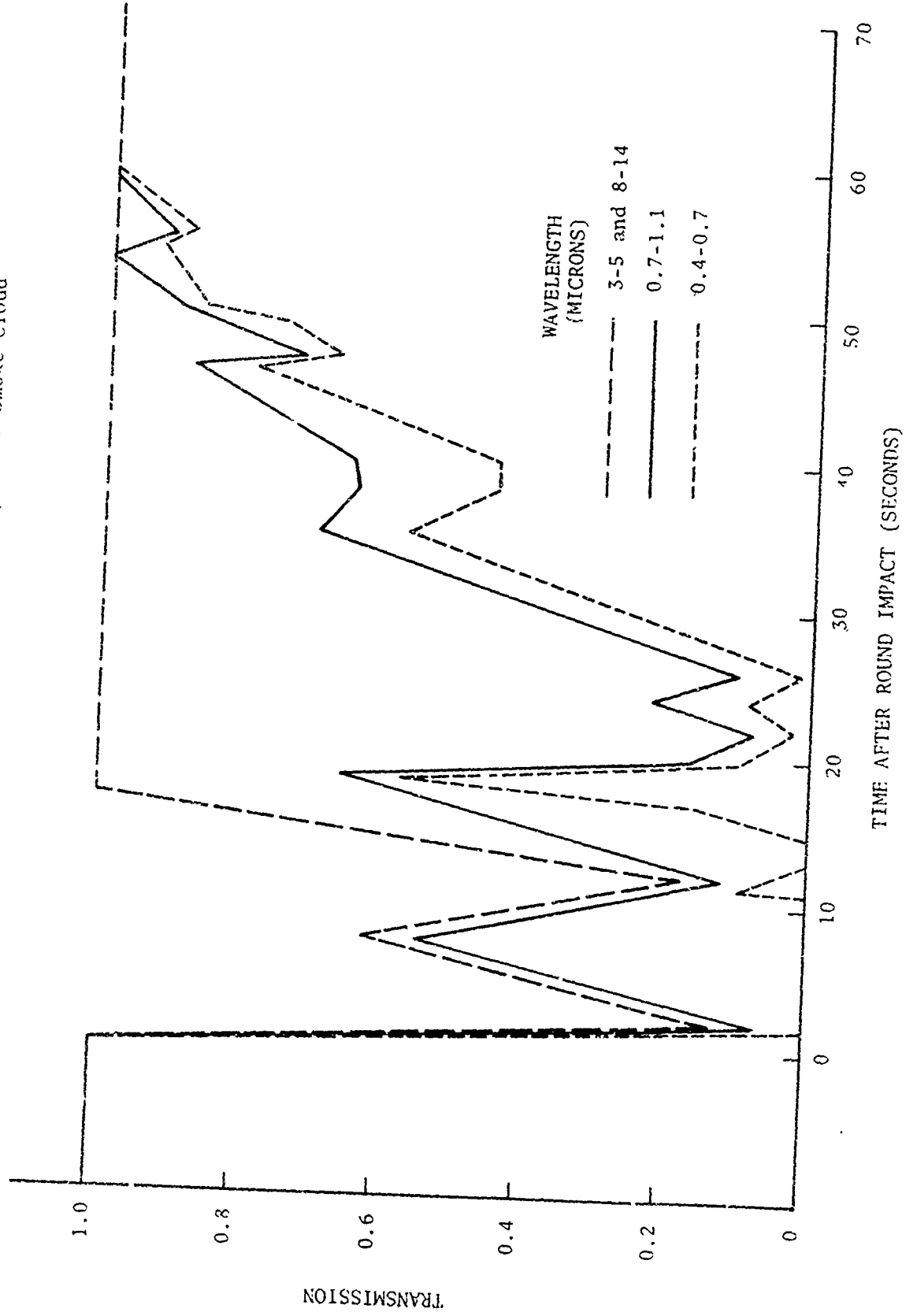
Figure 15. Optical Transmission Through a Fog Oil Smoke Cloud

42
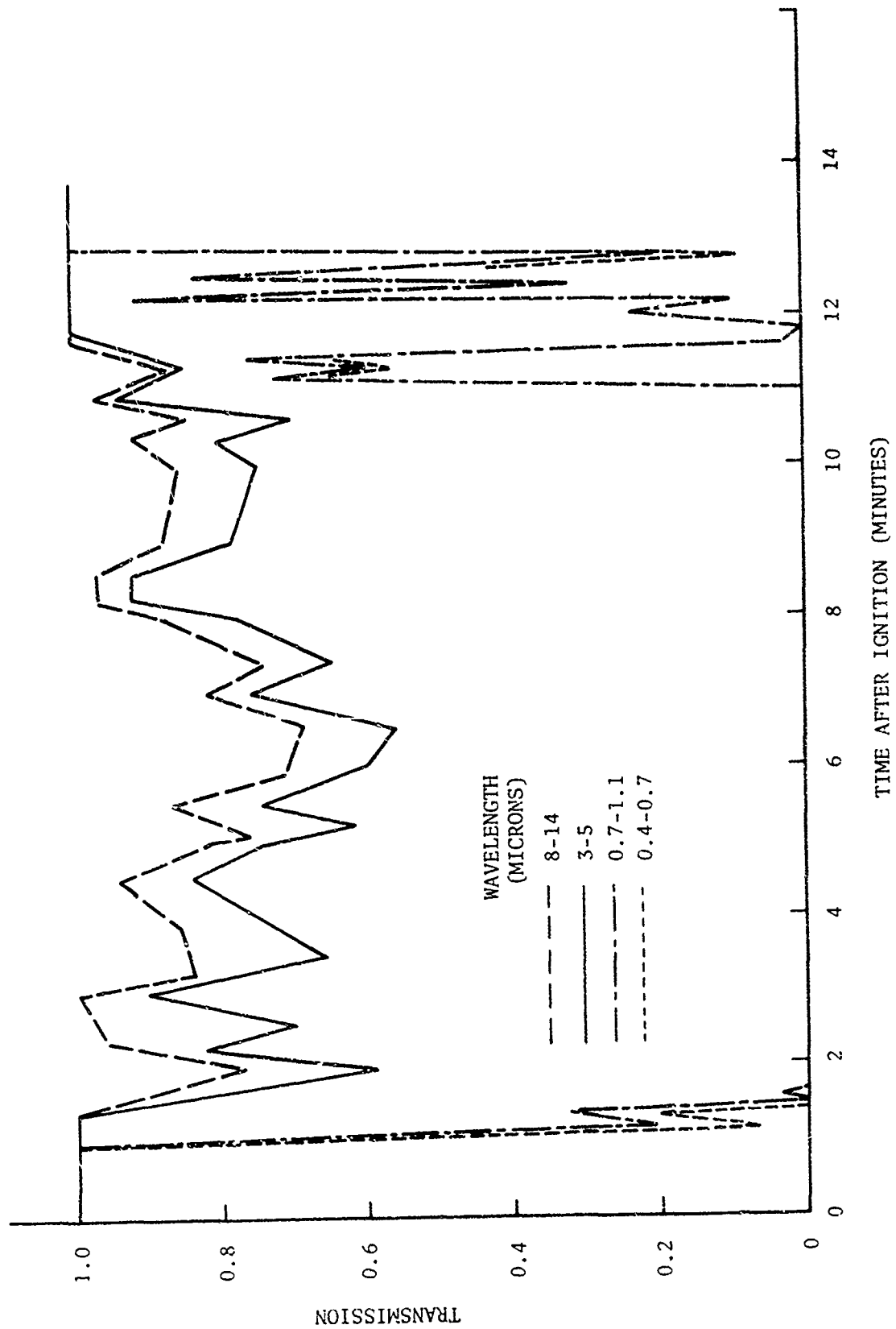
WAVELENGTH (MICRONS)	MEASURED QUANTITY	MUNITION TYPE			
		FOG OIL POTS	HC POTS	UK GRENADES	ROCKETS,MORTARS AND ARTILLERY PROJECTILES
0.4-0.7	Maximum Time of Total Attenuation	10	17	4	45
0.7-1.1	Maximum Time of Total Attenuation	10	17	4	43
3-5	Maximum Time of Total Attenuation	0	0	0	17
	Average Transmission	0.80	0.70	0.65	
	Minimum Transmission	0.35	0.15	0.05	0
8-14	Maximum Time of Total Attenuation	0	0	0	13
	Average Transmission	0.90	0.80	0.70	
	Minimum Transmission	0.50	0.35	0.15	0

The attenuation of radiation by dust is even more difficult to predict than is the case with smoke. Whereas battlefield smokes exhibit most of their attenuating effects through scattering, dust can make its contribution through both scattering and absorption. The relative importance of these mechanisms is also a function of both the particle size and chemical composition, which are dependent on both the geographical region and the ground condition. Furthermore, the wavelength dependence of the attenuation is even more complicated than in the case of smoke. Two examples of attenuation through dust caused by moving vehicles are shown in Figures 16 and 17. Figure 16 presents data which were collected at Fort Sill during a smoke test. The smoke effects are seen to the left; dust effects are shown on the right. Radio communication with the vehicle causing the dust interfered with the method of collecting the 3-5 and 8-14 micron data, so there is a break in the curve for these wavelengths. Figure 17 shows an independent dust measurement made during the APG tests. The 94- and 140-GHz radars were operated during this test and, again, no attenuation resulted from the dust at these frequencies.

43

Figure 16. Optical Transmission Through a Dust Cloud

WAVELENGTH
(MICRONS)

3-5 and 8-14

0.7-1.1

0.4-0.7

TRANSMISSION

TIME AFTER ROUND IMPACT (SECONDS)

44
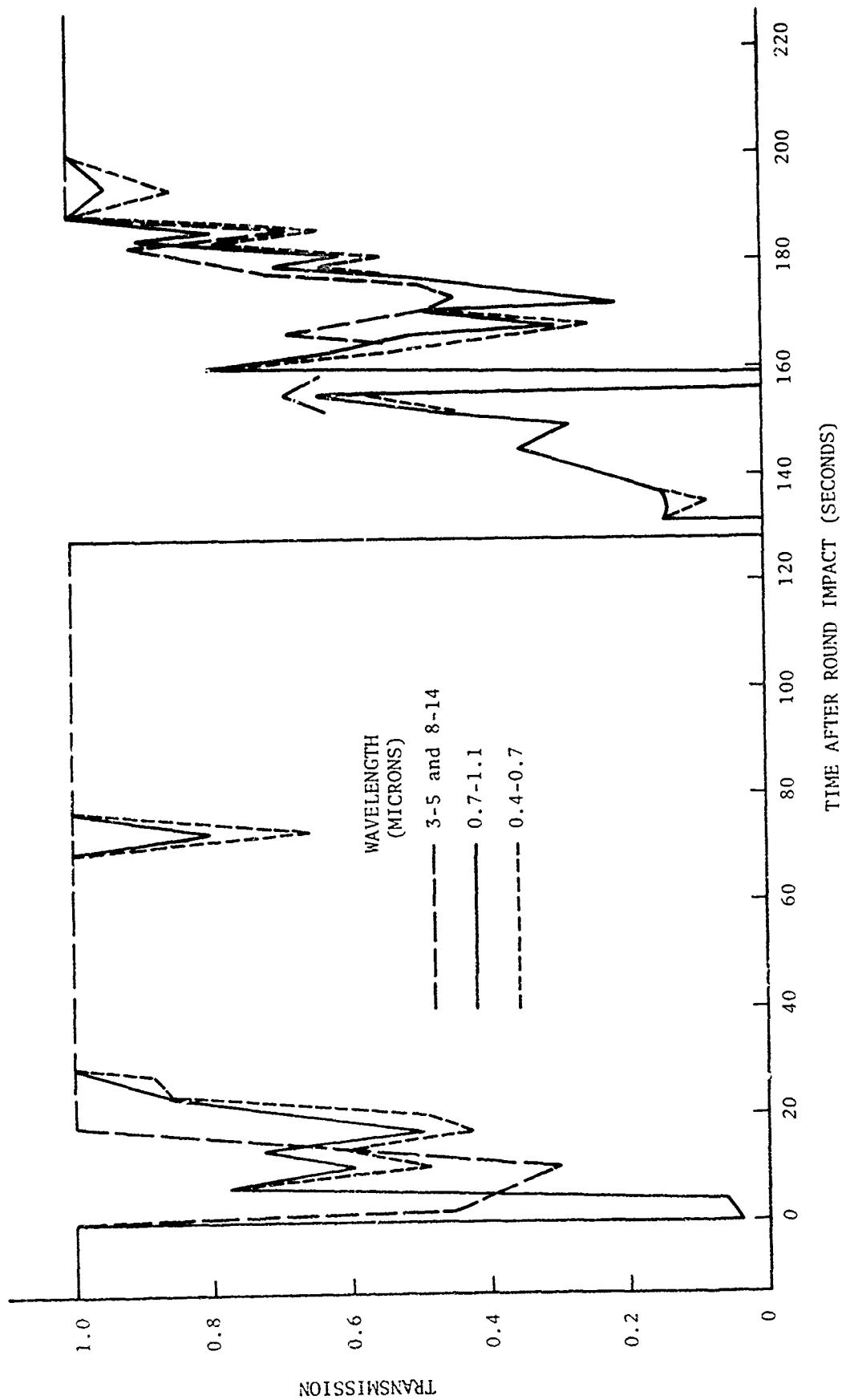
Figure 17. Optical Transmission Through a Dust Cloud

WAVELENGTH
(MICRONS)
8-14
3-5
0.7-1.1
0.4-0.7

TRANSMISSION

TIME (MINUTES)

45
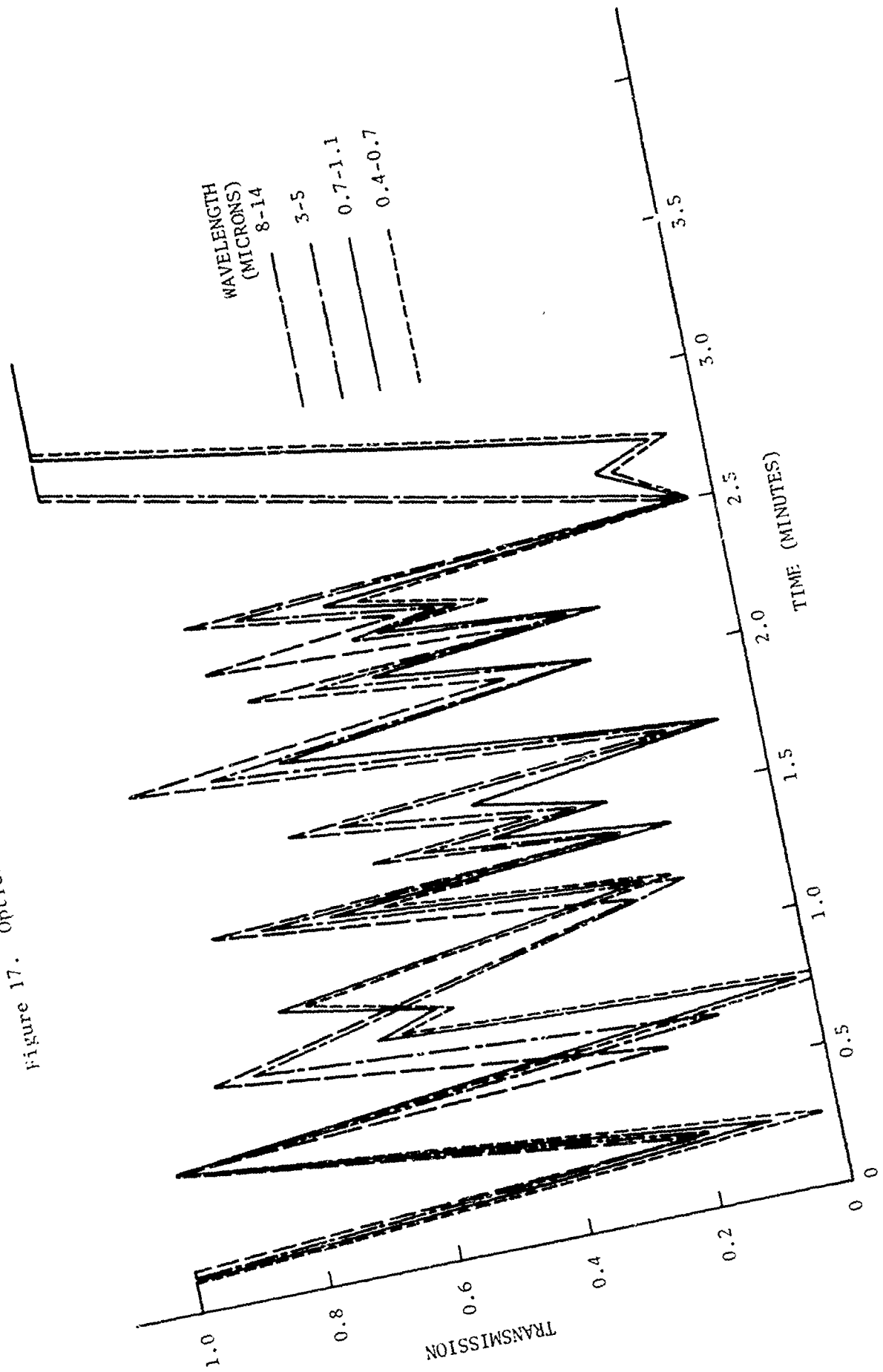
Other battlefield contaminants can also contribute to the attenuation in a tactical environment. Such contaminants might include hydrocarbons from vehicle emissions, gun firing by-products, and possibly effluents from cooking and heating sources as well. The effects of these contaminants are as difficult to predict as the effects of dust, and the data base needed to describe the transmission is virtually nonexistent.

III. APPLICATIONS

Before trying to solve a real transmission problem, it is desirable to simplify the process by consolidating the various pieces of information generated in Section II. The table and equations describing water vapor and carbon dioxide absorption in the optical region can be used as they stand. A single table can be generated for haze and fog by combining the tables describing the scattering and absorption coefficients and the continuum attenuation coefficient, where it applies. Another table can be generated to describe the attenuation coefficient of rain by consolidating the scattering and absorption tables pertaining to rain. The following two tables represent this consolidation.

The visibility of 326 km shown in the first table corresponds to the Rayleigh limit wherein the atmosphere consists of perfectly clear air with no water drops present.

The most general form of the equation describing the transmission between two points A and B through a medium characterized by an attenuation coefficient $\sigma(r)$ is

$$T = \exp\left[-\int_A^B \sigma(r)dr\right] . \tag{19}$$

It is frequently assumed that along a path parallel to the ground, the attenuation coefficient is independent of position. Although this is certainly not true in a smoke or dust environment, it is often sufficiently true when dealing with natural atmospheric constituents that Equation (19) can be reduced to

$$T = \exp(-R\sigma), \tag{20}$$

which is the form most often seen in atmospheric transmission literature. For the balance of this report it is assumed that σ is a constant in any horizontal plane, but it should be kept in mind that there are cases where that assumption is invalid and Equation (19) must be used.

46

HAZE AND FOG ATTENUATION COEFFICIENTS (KM^{-1})

VISIBILITY (KM)	WAVELENGTH (MICRONS)				
	0.55	1.06	2.3	3.8	10.6
0.1	3.8×10^1	3.8×10^1	3.8×10^1	4.0×10^1	1.3×10^2
0.2	2.2×10^1	2.2×10^1	2.1×10^1	2.0×10^1	6.5×10^1
0.5	9.5×10^0	9.5×10^0	8.7×10^0	7.1×10^0	1.7×10^1
1.0	4.8×10^0	4.8×10^0	4.4×10^0	3.5×10^0	4.4×10^0
2.0	2.2×10^0	2.2×10^0	1.9×10^0	1.6×10^0	1.2×10^0
5.0	5.5×10^{-1}	9.5×10^{-1}	8.5×10^{-1}	6.6×10^{-1}	3.1×10^{-1}
10.0	4.8×10^{-1}	4.8×10^{-1}	4.2×10^{-1}	3.3×10^{-1}	1.7×10^{-1}
20.0	2.4×10^{-1}	2.4×10^{-1}	2.1×10^{-1}	1.6×10^{-1}	9.4×10^{-2}
50.0	9.5×10^{-2}	9.5×10^{-2}	8.3×10^{-2}	6.1×10^{-2}	6.7×10^{-2}
326.0	1.2×10^{-2}	8.2×10^{-4}	3.7×10^{-5}	5.0×10^{-6}	8.0×10^{-8}

FREQUENCY (GHZ)				
9.375	35	94	140	240
0	1.6×10^{-2}	4.4×10^{-2}	3.2×10^{-1}	1.4×10^{-1}

47

RAIN ATTENUATION COEFFICIENT (KM^{-1})

RAINFALL RATE (MM/HR)	WAVELENGTH (MICRONS)					FREQUENCY (GHZ)				
	0.55	1.06	2.3	3.8	10.6	9.375	35	94	140	240
1	2.4×10^{-1}	2.5×10^{-1}	3.0×10^{-1}	3.1×10^{-1}	3.2×10^{-1}	2.1×10^{-3}	6.3×10^{-2}	2.6×10^{-1}	3.0×10^{-1}	3.0×10^{-1}
2	3.8×10^{-1}	3.9×10^{-1}	4.6×10^{-1}	4.7×10^{-1}	4.8×10^{-1}	5.0×10^{-3}	1.3×10^{-1}	4.6×10^{-1}	$4.7 \times 10^{-}$	4.7×10^{-1}
4	5.8×10^{-1}	6.0×10^{-1}	7.0×10^{-1}	7.2×10^{-1}	7.4×10^{-1}	1.2×10^{-2}	2.6×10^{-1}	7.6×10^{-1}	5×10^{-1}	7.5×10^{-1}
8	8.8×10^{-1}	9.2×10^{-1}	1.1×10^{0}	1.1×10^{0}	1.1×10^{0}	3.0×10^{-2}	4.8×10^{-1}	1.1×10^{0}	1.3×10^{0}	1.3×10^{0}
16	1.4×10^{0}	1.4×10^{1}	1.7×10^{0}	1.7×10^{0}	1.7×10^{0}	6.9×10^{-2}	9.6×10^{-1}	2.6×10^{0}	2.1×10^{0}	2.1×10^{0}
32	2.1×10^{0}	2.2×10^{1}	2.6×10^{0}	2.6×10^{0}	2.7×10^{0}	1.7×10^{-2}	1.8×10^{0}	3.3×10^{0}	3.5×10^{0}	3.5×10^{0}
64	3.2×10^{0}	3.4×10^{1}	4.0×10^{0}	4.0×10^{0}	4.1×10^{0}	4.1×10^{-1}	3.5×10^{0}	5.2×10^{0}	$5.$	5.5×10^{0}

If the radiation path is not in a horizontal plane but instead is inclined to the earth at an angle θ, Equation (18) must be employed. It is necessary in this case to determine the manner in which σ varies with altitude. Reference 27 contains an analysis of some available information on the altitude dependence of σ. Some of the results from that report can be summarized as follows. The decrease in the concentration of a particular atmospheric constituent with altitude can be described by

$$Z = Z_o e^{-h/s} = Z_o e^{-r \sin \theta/s}, \qquad (21)$$

where Z_o is the ground-level concentration and h is the altitude. S, a function of the constituent of interest, is called the scale height of that constituent and is the altitude at which the concentration decreases to 1/e, its ground level value. The gases comprising the atmosphere, and therefore the Rayleigh scattering coefficient, decrease with altitude in a very regular manner with a scale height of 8 km. The Rayleigh scattering coefficient is therefore given by

$$\sigma_R = \sigma_{R,o} e^{-r \sin \theta/8 \text{ km}}. \qquad (22)$$

The water vapor concentration is reasonably well behaved and exhibits a scale height of 2 km. The water vapor concentration expressed in cm per km of path length is therefore

$$W^* = W_o^* e^{-r \sin \theta/2 \text{ km}}. \qquad (23)$$

The Mie scattering coefficient, however, decreases with altitude in a manner which can only roughly be predicted. Its scale height, instead of being constant, is a function of the altitude, the visibility, and the wavelength of the radiation. The following expressions for σ are based on empirical data and are crude approximations to the σ-versus-altitude curves.

$$\left.\begin{array}{ll} \sigma_M = \sigma_{M,o} e^{-r \sin \theta/4.1 \text{ km}} & V \geq G(\lambda) \\[2ex] \sigma_M = \sigma_{M,o} e^{-r(\text{km}) \sin \theta \times \ln(0.1 \text{ km}^{-1}/\sigma_{M,o})} & V < G(\lambda), \ 0 < r \sin \theta < 1 \text{ km} \\[2ex] \sigma_M = 0.128 \text{ km}^{-1} e^{-r \sin \theta/4.1 \text{ km}} & V < G(\lambda), \ 1 \text{ km} < r \sin \theta < \infty \end{array}\right\} \quad (24)$$

[27] A.R. Downs, "A Model for Predicting the Spectral Irradiance on a Ground Target from the Sun and the Clear Daytime Sky," BRL Memo Report No. 2221, September 1972.

$G(\lambda)$ is given in Figure 18 for the visual and near infrared wavelengths. The shape of the curve at longer wavelengths is very uncertain, but there are some indications that it drops to a value of about 5 km at 10.6 microns.

Next, an example will be given describing how to make a transmission calculation. Let us assume an atmosphere with a visibility of 10 km, a temperature of 20°C, and a relative humidity of 80 percent. We wish to determine the transmission of a 1.06 micron laser beam between two points, one at ground level and the other, 7 km down-range and at an altitude of 3 km. From the first table in this section we find that $\sigma_o = 0.48$ km^{-1}. We also find from Figure 4 that $W^* = 1.24$ cm/km. From the geometry we find that the path length is 7.62 km and $\sin \theta = 0.394$. To find the amount of water vapor in the path, we integrate equation (21) in which S assumes the value of 2 km. The result i

$$W = 1.24 \int_0^{7.62} e^{-0.394\, r/2}\, dr = 4.89 \text{ cm.} \tag{25}$$

The transmission through the absorbing component of the atmosphere is now given by Equation (8) and

$$T = 1 - \text{erf}\, (0.22 \sqrt{4.89\pi}/2) = 0.458. \tag{26}$$

To obtain the scattering transmission we first note from Figure 18 that $G(\lambda) = 13$ km. Since this is greater than the visibility, the transmission must be calculated in two parts by using the last two expressions of Equation (24). The first part, which describes the transmission in the part of the atmosphere between altitudes of zero and 1 km, uses values of r between zero and 2.54 km. Equation (19) then shows the transmission to be

$$T = \exp\left[- 0.48 \int_0^{2.54} e^{0.394\ r \times \ln(0.1/0.48)}\, dr\right] = 0.541. \tag{27}$$

The transmission through the scattering component at altitudes above 1 km (r between 2.54 and 7.62 km) is calculated using Equation (19) and the third expression of Equation (23) resulting in

$$T = \exp\left[- 0.128 \int_{2.54}^{7.62} e^{-0.394\ r/4.1}\, dr\right] = 0.668. \tag{28}$$
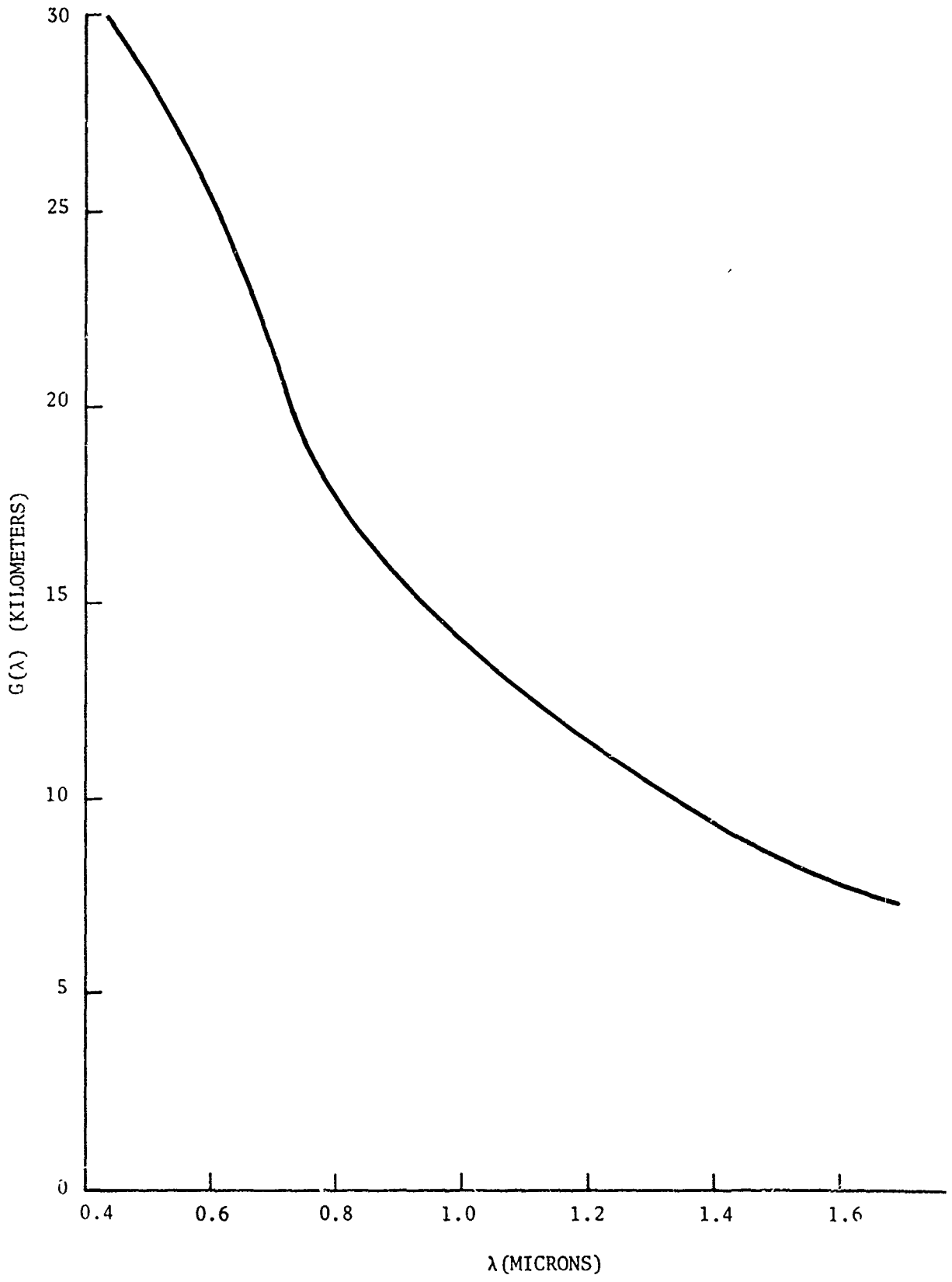
Figure 18. G(λ) as a Function of λ

The total transmission along the path is now the product of the partial transmissions given in Equations (26), (27), and (28) or 0.166.

Finally, a discussion of some limitations to imputs needed in the prediction of atmospheric transmission will be given. In the microwave region, two main problems are apparent. First is the lumping of the effects of air, water vapor, haze, and fog into a single continuum attenuation coefficient. Although the effect of these constituents is small, it would be desirable to have more hard data to document the situation more thoroughly. The other limitation pertains to the scattering and absorption coefficients in rain. Those given in this report are based on the drop radius distributions of Best.[20] It would be desirable to have data based on other distributions as well so that limits on the attenuation coefficients in rain of different rates can be specified.

In the optical region, a number of limitations are evident. To better calculate the attenuation by water vapor, a better attenuation model is needed for long wavelengths and absorption coefficients need to be measured using various laser lines as the radiation sources. Attenuation by haze and fog could be predicted more accurately if more data were available on droplet radius distributions covering a wider range of droplet sizes. If a spread of scattering coefficients in rain could be established which would cover the variation in the drop radius distribution for all types of rain, greater confidence in the predictions would result. Finally, absorption coefficients of liquid water at a larger number of wavelengths, particularly in regions of high transmission, would allow much better predictions of water drop absorption to be made.

REFERENCES

1. V.W. Richard and J.E. Kammerer, "Rain Backscatter Measurements and Theory at Millimeter Wavelengths," BRL Report No. 1838, October 1975. (AD #B008173L)

2. D.F. Fisher et al., "Transmissometry and Atmospheric-Transmission Studies - Final Report," University of Michigan, Institute of Science and Technology, March 1963.

3. J. McClatchey and J. Selby, "Atmospheric Transmittance from 0.25 to 28.5µm: Computer Code LOWTRAN 3", AFCRL-TR-75-0255, May 1975.

4. G.Mie, "Beitrage zer Optik Truber Medien, Speziell Kolloidales Metallosungen," Ann. der Phys., Vol. 25, 1908.

5. E.J. McCartney, "Scattering - The Interaction of Light and Matter," Sperry Report No. AB-1272-0057, February 1966.

6. J. Stephenson, W. Haseltine, and C. Moore, Atmospheric Absorption of CO_2 Laser Radiation," Applied Physics Letters, Vol. 11, No. 5, September 1967.

7. T. Elder and J. Strong, "The Infrared Transmission of Atmospheric Windows," J. Franklin Inst., Vol. 255, No. 3 (1953).

8. W.M. Elsasser, "Heat Transfer by Infrared Radiation in the Atmosphere," Harvard Meteorological Series 6, Harvard University Press, Cambridge, Massachusetts, 1942.

9. Henry L. Hackforth, Infrared Radiation, McGraw-Hill Book Company, Inc., 1960.

10. J. McCoy, D. Rensch, and R. Long, "Water Vapor Continuum Absorption of Carbon Dioxide Laser Radiation Near 10," Applied Optics, Vol. 8, No. 7, 1969.

11. D.E. Gray, ed. American Institute of Physics Handbook, Second Edition, McGraw-Hill Book Company, Inc., 1963.

12. W.E.K. Middleton, Vision Through the Atmosphere, University of Toronto Press, Toronto, Canada, 1952.

13. H.G. Houghton and W.R. Chalker, "Scattering Cross Sections of Water Drops in Air for Visible Light," JOSA, Vol. 39, No. 11, November 1949.

14. J.J. Stephens, "Radar Cross-Sections for Water and Ice Spheres," J. of Meteorology, Vol. 18, 1961.

15. D.H. Dickson, R.B. Loveland, and W.H. Hatch, "Atmospheric Waterdrop Size Distribution at Capistrano Test Site (CTS) From 16 April Through 11 May 1974 - Vols. IV and V," U.S. Army Atmospheric Sciences Laboratory Report ECOM-DR-75-3, September 1975.

16. H. Dessens, "Brume et Noyaux de Condensation," Ann de Géophys., Vol. 3, 1947.

17. R.S. Sekhon and R.C. Srivastava, "Doppler Radar Observations of Drop-Size Distribution in a Thunderstorm," J. Atm. Sci., Vol. 28, No. 6, September 1971.

18. J.S. Marshall and W.M. Palmer, "The Distribution of Raindrops with Size," Journal of Meteorology, Vol. 15, August 1948.

19. J.O. Laws and D.A. Parsons, "The Relation of Raindrop-Size to Intensity," Transactions, American Geophysical Society, Vol. 24, Part 2, 1943.

20. A.C. Best, "The Size Distribution of Raindrops," Quarterly Journal Royal Meteorological Society, Vol. 76, 1950.

21. A.R. Downs, "A Model for Predicting the Rain Backscatter from a 70 GHz Radar," BRL Memo Report No. 2467, March 1975. (AD #A009699)

22. D.E. Setzer, "Computed Transmission Through Rain at Microwave and Visible Frequencies," BSTJ, Vol. 49, 1970.

23. G. Zanotelli, "Assorbimento Elementare Della Luce nel Passagio Attraverso Alle Nubi," Atti. Accad. Ital., Rend. Cl. Sci. Fis. Mat. Nat., Vol. 2, 1940.

24. D. Deirmendjian, Electromagnetic Scattering on Spherical Polydispersions, American Elsevier Publishing Company, Inc., New York, 1969.

25. G. Allen and B. Simonson, "Attenuation of Infrared Laser Radiation by HC, FS, WP, and Fog Oil Smokes," Edgewood Arsenal Technical Report EATR 4405, May 1970.

26. R.G. Reitz, "An Analysis of Smoke Transmission Measurements and Techniques," BRL Memorandum Report (in preparation).

27. A.R. Downs, "A Model for Predicting the Spectral Irradiance on a Ground Target from the Sun and the Clear Daytime Sky," BRL Memo Report No. 2221, September 1972.

DISTRIBUTION LIST

No. of Copies	Organization	No. of Copies	Organization

12 Commander
Defense Documentation Center
ATTN: DDC-TCA
Cameron Station
Alexandria, VA   22314

1 Director
Defense Advanced Research
   Projects Agency
ATTN: Dr. L. Strom
1400 Wilson Boulevard
Arlington, VA   22209

1 Director
Institute for Defense Analysis
400 Army-Navy Drive
Arlington, VA   22202

1 Commander
US Army Materiel Development
   and Readiness Command
ATTN: DRCDMA-ST
5001 Eisenhower Avenue
Alexandria, VA   22333

1 Commander
US Army Aviation Systems
   Command
ATTN: DRSAV-E
12th and Spruce Streets
St. Louis, MO   63166

1 Director
US Army Air Mobility Research
   and Development Laboratory
Ames Research Center
Moffett Field, CA   94035

6 Commander
US Army Electronics Command
ATTN: DRSEL-RD
      DRSEL-CT-LB,
         Mr. Anthony J. Carillo
         Mr. Frank J. Elmer
      DRSEL-TL-I, Dr. Jacobs
      DRSEL-CT-R, Mr. Pearce
      DRSEL-CT-L-A,
         Mr. R. Tuttle
Fort Monmouth, NJ   07703

3 Commander/Director
Atmospheric Sciences Laboratory
ATTN: DRSEL-BL-RA,
         Dr. Howard Holt
         Mr. James Mason
      DRSEL-WLM-ST,
         Mr. Robert Clawson
White Sands Missile Range, NM
88002

1 Commander
US Army Electronics Research
   and Development Activity
ATTN: DRSEL-WL-MT, R. Murray
White Sands Missile Range, NM
88002

2 Director
US Army Night Vision Laboratory
Visionics Technical Area
ATTN: DRSEL-NV-VI,
         Mr. Neil Sherman
         Mr. Ferdinand Zegel
Fort Belvoir, VA   22060

No. of Copies	Organization	No. of Copies	Organization
5	Commander US Army Missile Command ATTN: DRSMI-R DRSMI-RE, Mr. Ray Farmer Dr. J. Whitney Blanchard Mr. W. J. Lindberg DRSMI-RES, Mr. John French Redstone Arsenal, AL 35809	2	Commander US Army Rock Island Arsenal ATTN: SARRI-LR, Mr. M. Amoruso LT Steven Babiak Rock Island, IL 61201
2	Commander US Army Tank Automotive Development Command ATTN: DRDTA-RWL DRDTA-RGD, D. Wilburn Warren, MI 48090	3	Commander US Army Harry Diamond Laboratories ATTN: DRXDO-TI DRXDO-TD/002 DRXDO-RA, J. Salerno 2800 Powder Mill Road Adelphi, MD 20783
3	Commander US Army Mobility Equipment Research & Development Center ATTN: Tech Docu Cen, Bldg. 315 DRSME-RZT STSFB-MB, Mr. A. Perri Fort Belvoir, VA 22060	1	Commander US Army Foreign Science and Technology Center ATTN: DRXST-CB3, Mr. D. Hardin Federal Office Building 220 7th Street, NE Charlottesville, VA 22901
3	Commander US Army Armament Command ATTN: DRSAR-RD, J.A. Brinkman DRSAR-RDR, Dr. R. Moore Mr. Jack Turkeltaub Rock Island, IL 61202	2	ARADCOM ATTN: DRCPM-CAWS, LTC Robert Nulk Dr. William Barrett Dover, NJ 07801
1	Commander US Army Frankford Arsenal ATTN: Mr. Robert Pfeilsticker (N600) Philadelphia, PA 19137	1	Commander US Army Training & Doctrine Command ATTN: ATCD-CF, CPT D.C. Gunn Fort Monroe, VA
4	Commander US Army Picatinny Arsenal ATTN: SARPA-FR-L, Mr. Paul J. Kisatsky Mr. Matt Nowak SARPA-DW12, T. Malgeri SARPA-ND-C, Mr. Leonard Nichols Dover, NJ 07801	1	Director US Army TRADOC Systems Analysis Activity ATTN: ATAA-SA White Sands Missile Range, NM 88002
		1	Commander US Army Field Artillery School ATTN: ATSF-CD-DA, CPT Antoniotti Fort Sill, OK 73503

No. of Copies	Organization	No. of Copies	Organization
1	Office of Assistant Secretary of the Army for R&D ATTN: Assistant for Electronics Mr. Victor Friedrich Washington, DC 20310	1	Commander US Naval Weapons Center ATTN: Dr. J. Battles, Code 6014 China Lake, CA 93555
1	HQDA (DAMA-ART-B, LTC N. Conner) Washington, DC 20310	1	Commander US Naval Research Laboratory ATTN: Radar Div, Dr. Sholnik Washington, DC 20375
1	HQDA (DAMA-ARZ-B, Dr. Watson) Washington, DC 20310	1	AFATL (DLMM, F.H. Prestwood) Eglin AFB, FL 32542
1	Commander US Army Research Office ATTN: Dr. D. Van Huisteyn P. O. Box 12211 Research Triangle Park NC 27709	1	RADC (OCSF, R. Polce) Griffiss AFB, NY 13411
		1	AFGL/LZ (Mr. C. Sletten) Hanscom AFB, MA 01731
1	Commander US Army Communications Electronics Engineering Installation Agency ATTN: SCC-CED-RD, MAJ Carre Fort Huachuca, AR 85613	1	AFAL (WRP, Mr. Leasure) Wright-Patterson AFB, OH 45433
		1	AFWL (TEM-4, Mr. J. Schell) Wright-Patterson AFB, OH 45433
1	Director US Army Engineer Waterways Experiment Station ATTN: Mr. Lewis Decell P.O. Box 631 Vicksburg, MS 39180	1	Director National Oceanic and Atmospheric Administration Environmental Research Laboratories ATTN: Code R42 US Department of Commerce Boulder, CO 80302
2	Commander US Naval Air Development Center ATTN: AFTD, Radar Division Mr. M. Foral Warminster, PA 18974	2	Director Office of Telecommunications Institute for Telecommunications Sciences ATTN: Dr. H.J. Liebe Dr. L. Wood Boulder, CO 80302
1	Commander US Naval Electronics Lab Center ATTN: Mr. J.H. Provencher, Code 2330 San Diego, CA 92152		

No. of Copies	Organization	No. of Copies	Organization
1	Energy Research and Development Administration Dept. of Military Applications Biomedical & Environmental Research Division ATTN: Mr. Robert Beadle Washington, DC 20545	1	Hughes Aircraft Company Aerospace Group Advanced Program Development Systems Division ATTN: P.B. Reggie Canoga Park, CA 91304
1	Director NASA Goddard Space Flight Center ATTN: Mr. L.J. Ippolito, Code 951 Greenbelt, MD 20771	1	Hughes Aircraft Company Electron Dynamic Division ATTN: Mr. N.B. Kramer 3100 West Lomita Blvd Torrance, CA 90504
1	Aerospace Corporation Electronics Research Laboratory El Segundo Technical Operations ATTN: Dr. R.L. Mitchell P.O. Box 95085 Los Angeles, CA 90045	1	Hughes Aircraft Company Radar Division ATTN: Mr. John Haney Culver City, CA 90230
1	Bell Telephone Laboratories Crawford Hill Laboratory ATTN: Mr. D.C. Hogg Holmdel, NJ 07733	1	Illinois State Water Survey ATTN: Mr. Richard Semonin Box 232 Urbana, IL 61801
1	Boeing Aircraft Company Boeing Aerospace Division ATTN: Mr. Jim Rowley Mail Stop 86-04 Department 2-5160 Kent, WA 98370	1	LTV Aerospace Corporation Michigan Division ATTN: Dr. J. Mayersak P.O. Box 909 Warren, MI 48090
1	Goodyear Aerospace Corporation Arizona Division ATTN: Mr. Fred Wilcox Litchfield Park, AZ 85340	1	Martin Marietta Corporation ATTN: Mr. Jim Wiltse Orlanda, FL 32805
1	Honeywell Incorporated Systems & Research Division ATTN: Mr. Ray Zirkle 2700 Ridgway Parkway Minneapolis, MN 55413	1	Norden Division United Aircraft Corporation ATTN: Dr. L. Kosowsky Helen Street Norwalk, CT 06852
		1	The Rand Corporation ATTN: Dr. S.J. Dudzinsky, Jr. 1700 Main Street Santa Monica, CA 90406

No. of Copies	Organization
1	Raytheon Company Missiles Systems Division ATTN: Mr. Walter Justice Hartwell Road Bedford, MA 01730
2	Sperry Rand Corporation ATTN: Mr. James Cleotelis Mr. R. Roder P.O. Box 4648 Clearwater, FL 33518
1	Technology Service Corporation ATTN: Dr. Fred Nathanson Santa Monica, CA 90401
1	Arizona State University Electrical Engineering Dept. ATTN: Dr. Murray Circus Phoenix, AZ 85026
1	Georgia Institute of Technology Engineering Research Building ATTN: Dr. R. Hayes 347 Ferst Drive Atlanta, GA 30332
1	John Hopkins University Applied Physics Laboratory ATTN: Ray Harris Johns Hopkins Road Laurel, MD 20810
2	Director MIT Lincoln Laboratory ATTN: Dr. Thomas Johns Dr. R. K. Crane 244 Wood Street Lexington, MA 02173
1	South Dakota School of Mines and Technology ATTN: Dr. Paul Smith Rapid City, SD 57701

No. of Copies	Organization
1	Syracuse University Department of Electrical Engineering ATTN: Dr. R. McFee Syracuse, NY 13210
1	University of Alabama Institute of Atmospheric Physics ATTN: Dr. L.J. Battan Tucson, AZ 85721
1	University of Miami Department of Meteorology ATTN: Prof. R. Lhermitte Coral Gables, FL 33134
2	University of Texas at Austin Electrical Engineering Research Laboratory ATTN: Dr. Archie Straiton Dr. Robert Fannin Rt. 4, Box 198 Austin, TX 78751
1	University of Washington College of Engineering Department of Electrical Engineering ATTN: Dr. James C. Lin Seattle, WA 98145

Aberdeen Proving Ground

Marine Corps Ln Ofc
Dir, USAMSAA
  ATTN: DRXSY-D, Dr. Sperrazza
        DRXSY-GM, G. Stiles
        DRXSY-GS, Mr. D. Barnhart
Cmdr, USAEA
  ATTN: SAREA-DE-MM,
        Mr. D. Anderson
Cmdr, USATECOM
  ATTN: DRSTE-ME, Dr. N. Pentz